SANDIA REPORT

SAND2001-3846
Unlimited Release
Printed December 2001

Evaluation of Impact Damage to the Burster Detonation Vessel Caused by Fragments from a Drained M121A1 Chemical Munition Detonated with an Initiation Charge

Marlin E. Kipp

Prepared by
Sandia National Laboratories
Albuquerque, New Mexico 87185 and Livermore, California 94550

Sandia is a multiprogram laboratory operated by Sandia Corporation,
a Lockheed Martin Company, for the United States Department of Energy under Contract DE-AC04-94AL85000.

Issued by Sandia National Laboratories, operated for the United States Department of Energy by Sandia Corporation.

Available to DOE and DOE contractors from
U.S. Department of Energy
Office of Scientific and Technical Information
P.O. Box 62
Oak Ridge, TN 37831

Telephone: (865)576-8401
Facsimile: (865)576-5728
E-Mail: reports@adonis.osti.gov
Online ordering: http://www.doe.gov/bridge

Available to the public from
U.S. Department of Commerce
National Technical Information Service
5285 Port Royal Rd
Springfield, VA 22161

Telephone: (800)553-6847
Facsimile: (703)605-6900
E-Mail: orders@ntis.fedworld.gov
Online order: http://www.ntis.gov/ordering.htm

SAND2001-3846
Unlimited Release
Printed December 2001

Evaluation of Impact Damage to the Burster Detonation Vessel Caused by Fragments from a Drained M121A1 Chemical Munition Detonated with an Initiation Charge

Marlin E. Kipp
Computational Physics and Simulation Frameworks Department
Sandia National Laboratories
P.O. Box 5800
Albuquerque, NM 87185-0820

ABSTRACT

Explosive charges placed on the fuze end of a drained chemical munition are expected to be used as a means to destroy the fuze and burster charges of the munition. Analyses are presented to evaluate the effect of these additional initiation charges on the fragmentation characteristics for the M121A1 155mm chemical munition, modeled with a T244 fuze attached, and to assess the consequences of these fragment impacts on the walls of a containment chamber – the Burster Detonation Vessel. A numerical shock physics code (CTH) is used to characterize the mass and velocity of munition fragments. Both two- and three-dimensional simulations of the munition have been completed in this study. Based on threshold fragment velocity / mass results drawn from both previous and current analyses, it is determined that under all fragment impact conditions from the munition configurations considered in this study, no perforation of the inner chamber wall will occur, and the integrity of the Burster Detonation Vessel is retained. However, the munition case fragments have sufficient mass and velocity to locally damage the surface of the inner wall of the containment vessel.

EXECUTIVE SUMMARY

Explosive charges placed on the fuze end of a drained chemical munition are expected to be used as a means to destroy the fuze and burster charges of the munition. Analyses are presented to evaluate the effect of these additional initiation charges on the fragmentation characteristics for the M121A1 155mm chemical munition, modeled with a T244 fuze attached, and to assess the consequences of these fragment impacts on the walls of a containment chamber – the Burster Detonation Vessel. A numerical shock physics code (CTH) is used to model the detonation of the M121A1 burster charge and the effects of additional initiation charge configurations. Both two- and three-dimensional simulations of the munition have been completed in this study. Fragment characteristics - mass and velocity - of munition fragments are obtained from the code calculations, in conjunction with the application of a fragmentation model that estimates fragment size from the local strain rate in the munition case. These fragments are compared with threshold fragment velocity / mass results drawn from both previous and current analyses. It is determined that under all fragment impact conditions from the munition configurations considered in this study, no perforation of the inner chamber wall will occur, and the integrity of the Burster Detonation Vessel is retained. However, the munition case fragments have sufficient mass and velocity to locally damage the surface of the inner wall of the containment vessel.

Several options for placement of a C-4 initiation charge near the nose were considered, including a single block, two blocks stacked atop one another, and two blocks symmetrically placed on opposite sides of the nose. Based on explosive models in the code simulations, it is found that these additional C-4 explosive initiation charges are sufficient to detonate both the fuze and burster charges. The additional explosive in the nose region only modifies the fragment formation and increases fragment velocities local to the site of the charge. The main burster charge for the M121A1 extends the full length of the munition, and remains the primary energy source for all the large fragments. As in previous analyses of this munition for chamber walls of comparable thickness, the fragments formed have insufficient velocity – mass combinations to perforate the 40 mm wall of the Burster Detonation Vessel.

ACKNOWLEDGMENTS

The authors gratefully acknowledge the support that Don Benton, NSCMP, Aberdeen Proving Ground, provided during the course of this study. The project oversight of Ken Tschritter, Sandia National Laboratories, Livermore, is much appreciated. Reviews by D. Benton, G. Bessette, and J. Stofleth proved very helpful with suggestions for clarifying the manuscript.

CONTENTS **Page**

I. INTRODUCTION

The United States Army is currently building a facility called the Munitions Assessment and Processing System (MAPS) at Aberdeen Proving Ground in Maryland. MAPS will support environmental restoration efforts by providing a facility to treat explosively configured chemical and smoke munitions by means other than open detonation. Specifically, chemical and smoke munitions will be drained of their liquid payload and decontaminated. Then the empty munition will be placed in a non-vented chamber called the Burster Detonation Vessel (BDV). An explosive charge is then placed on the fuze end of the munition to destroy the fuze and detonate the burster charge, thus eliminating the explosive hazard. The Burster Detonation Vessel (BDV) has been designed to sustain detonation of an uncased explosive mass that is significantly larger than any expected charge mass in the inventory to be demilitarized, as well as contain fragments without being breached. Previous analyses evaluated the effects of initiation point of the burster charge (without a fuze) and the presence or absence of agent on the fragment characteristics (Kipp, et al., 1999; Kipp and Martinez, 2000). Munitions representing a wide range of size and explosive burster charge mass were considered in those studies: M426 (8 inch), M121A1 (155 mm), Livens projectile, 4.2 inch mortar, Stokes mortar, and 75 mm chemical rounds. It was concluded from those analyses that fragments from all the listed chemical rounds were fully contained by chambers with walls of nominal 30 mm thickness. The current study is motivated by the need to ascertain the effect of the additional initiation charges on the fragment characteristics of the M121A1 munition, and the impact consequences to a comparable containment chamber wall. The M121A1 contains the largest expected explosive burster charge and is expected to generate the most damaging fragments to be encountered in this chamber.

When the chemical munitions were analyzed in the previously noted studies, the primary focus was on the effects of the burster charge on fragment formation, and no fuze was included in the models. In addition, all the configurations were axi-symmetric, so two-dimensional simulations were adequate to determine the initial motion induced by the burster explosive, and evaluate the fragment formation characteristics. In the present drained condition, deliberate detonation of the M121A1 with C-4 initiation charges is considered. A representation of the T244 fuze is included in the current model of the M121A1. The initiation charges are expected to be blocks of C-4 attached near the nose of the projectile. Depending upon how the C-4 is molded to the nose, this aspect of the configuration may no longer be axi-symmetric. To accommodate such possibilities, a few three-dimensional simulations were made to assess the effects of the added explosive on fragmentation.

The numerical simulations of the munition detonation were made with the CTH Eulerian shock wave propagation code (McGlaun, et al., 1990). This multi-dimensional shock physics Eulerian code, developed and maintained at Sandia National Laboratories, has the capability to model dynamic events that include explosive detonation and high velocity impact. The CTH code solves the differential equations describing conservation of mass, momentum and energy during transient dynamic events on a fixed spatial mesh. CTH is capable of tracking the interactions of up to 20 materials. This code contains models suitable to describe material response under most conditions encountered in shock physics, including the explosives and inert solids for the current application. A variety of material insert geometries facilitate the modeling of complex devices. The Eulerian structure of the code permits large deformations associated with explosive or impact events to be accommodated. The characteristic fragment dimensions in

the numerical simulations are determined by the strain rate, $\dot{e}$, at the time of fracture. The basic relationships between the strain rate and the fragment dimensions that result as materials fracture under high strain rate loading conditions have been derived by Grady (1988). In the current analyses, the temperature and strain rate regimes are such that the fragmentation is governed by the fracture toughness, K_C, of the steel. The average fragment size, S, is determined from

$$S = \left(\frac{\sqrt{24} K_C}{r c \dot{e}} \right)^{2/3} \tag{1}$$

where ρ is the density, and c is the sound speed (Grady, 1988). This fragment information is evaluated in the simulation, but does not couple back into the calculation to form discrete fragments (Kipp, et al., 1993; Appendix A, Kipp, et al., 1999). As the munition case expands radially outwards, driven by the burster explosive products, the divergent motion induces a circumferential (hoop) strain rate – basically the expansion velocity divided by the radial distance to the center of curvature, V_R/R. This strain rate determines the circumferential characteristic widths of the munition case fragments. The longitudinal strain rates are typically much smaller than the circumferential ones, leading to larger axial dimensions of the fragments, including potential strip-like features. This effect is commonly observed in framing camera records of explosively fragmenting cylinders, where the longitudinal fractures (formed by circumferential failure) are the first to appear (e.g., Wilson, et al., 2001).

An accurate determination of what would be considered the most damaging fragment from the munition detonation presents the most difficulties in such a study as this. The incident velocities of the case fragments can be fairly well bounded for the burster explosive employed in this munition. The CTH code calculations, Gurney methods (Jones, et al., 1980; Kennedy, 1970), and the empirical code, ConWep (ConWep, 1989) have been shown to give similar amplitudes for the source velocities (Kipp, et al., 1999). During the two previous studies, no arena test data were available to compare with the fragment dimensions obtained from the simulations, so strong reliance on analytic measures and related empirical data was required. Recent searches have recovered limited archival fragmentation arena data for the M121A1 that are compared to the computational estimates (Whitney, et al., 1983). In addition, recent comparisons of this fragmentation model with data from cylindrical test configurations have demonstrated excellent agreement (Wilson, et al., 2001). Accurate estimates of perforation thresholds are difficult to determine. Again, in the absence of target-specific data, a limit velocity curve is used that is based on an analytic function for long-rod penetration.

In the following sections, the containment vessel and M121A1 munition configurations are defined (Section II), including placement options of the initiation charges on the M121A1. In Section III, baseline simulations of the fuzed M121A1 without any C-4 are reviewed, followed by simulations of the munition with the C-4 attached – both one- and two-block options. In this latter section, the focus is on characterizing the expected fragments from the M121A1 munition. Consequences of fragment impacts on the Burster Detonation Vessel wall structure are discussed in Section IV. The material parameters used in the CTH calculations are tabulated in Appendix A. A determination of the limit velocity curve for the perforation threshold of the Burster Detonation Vessel is found in Appendix B. Although analysis of the exploding M121A1

munition is the focus of the main body of the report (Section III), summary results drawn from Kipp and Martinez (2000) for four other drained munitions - Livens projectile, 4.2 inch mortar, Stokes mortar, and 75 mm Mk II - are included in Appendix C.

II. GEOMETRY

The configurations of the Burster Detonation Vessel (BDV) and M121A1 chemical munition are described in this section. The BDV is a very complex device, with many external appendages. However, the interior exposed to the fragments is basically a simple curved wall. The focus was on determining the fragment characteristics created by the explosive source, and consequences of fragments that had unobstructed paths to impact the BDV wall as representing the worst case scenario.

A. Burster Detonation Vessel (BDV)

The Burster Detonation Vessel (BDV) is the primary containment device that must retain its integrity in this prescribed detonation event. A drawing of the BDV is shown in Figure 1 (Dynasafe, 2000). The internal diameter of the main chamber at the mid-plane is 1200 mm. Except for a short cylindrical region at the mid-plane, the main walls of the vessel are spherical, as shown in this drawing, and were originally to be constructed with an interior steel layer 30 mm thick, and an exterior steel wall also of thickness 30 mm, separated by a 5 mm air gap. A recent change to the design increases the thickness of both walls to 40 mm, retaining the original interior dimensions.

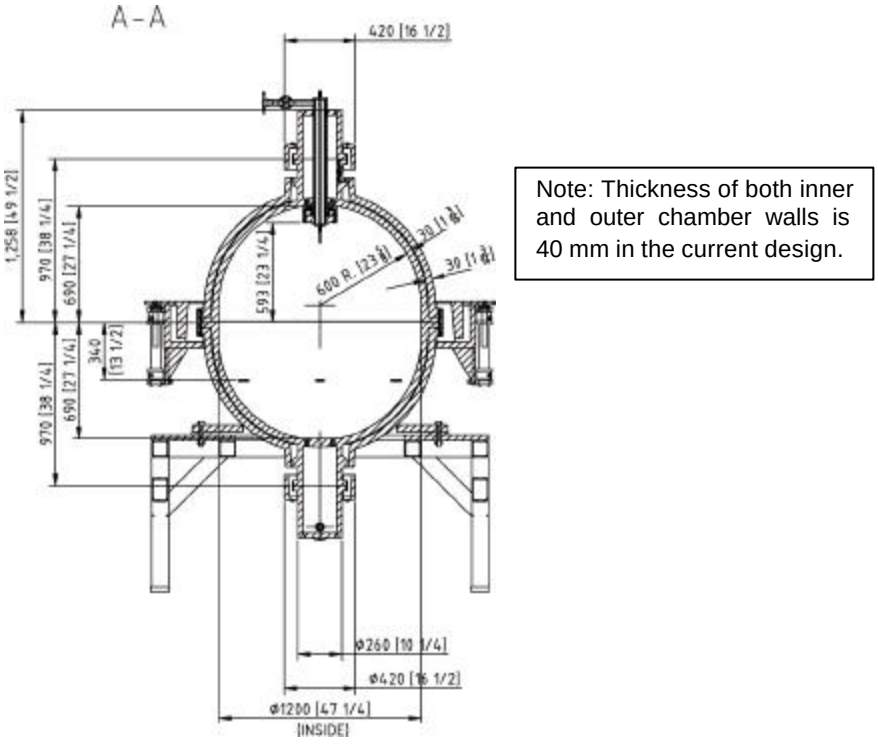

Figure 1. The basic design of the Burster Detonation Vessel (Dimensions in mm [inches]).

The chamber walls are constructed of cast stainless steel, S 165 M, manufactured by Scana Steel Stavanger A/S. The following properties of this steel are given by Hilding and Nilsson (2001): density, 7800 kg/m^3; Young's modulus, 210 N/mm^2; Poisson's ratio, 0.29; yield strength, 620 – 746 N/mm^2; tensile strength, 830 – 900 N/mm^2; and elongation to failure, 15 – 19 %. The proof testing of this structure to specified charge masses has been evaluated by the vessel manufacturer (Dynasafe), and is not a part of the present study.

B. M121A1 (155 mm) Chemical Munition / C-4 Initiation Charges

The M121A1 chemical round is a heavily cased 155 mm munition. The design of the projectile, from an assembly drawing, is shown in Figure 2 (Picatinny Arsenal, 1961a).

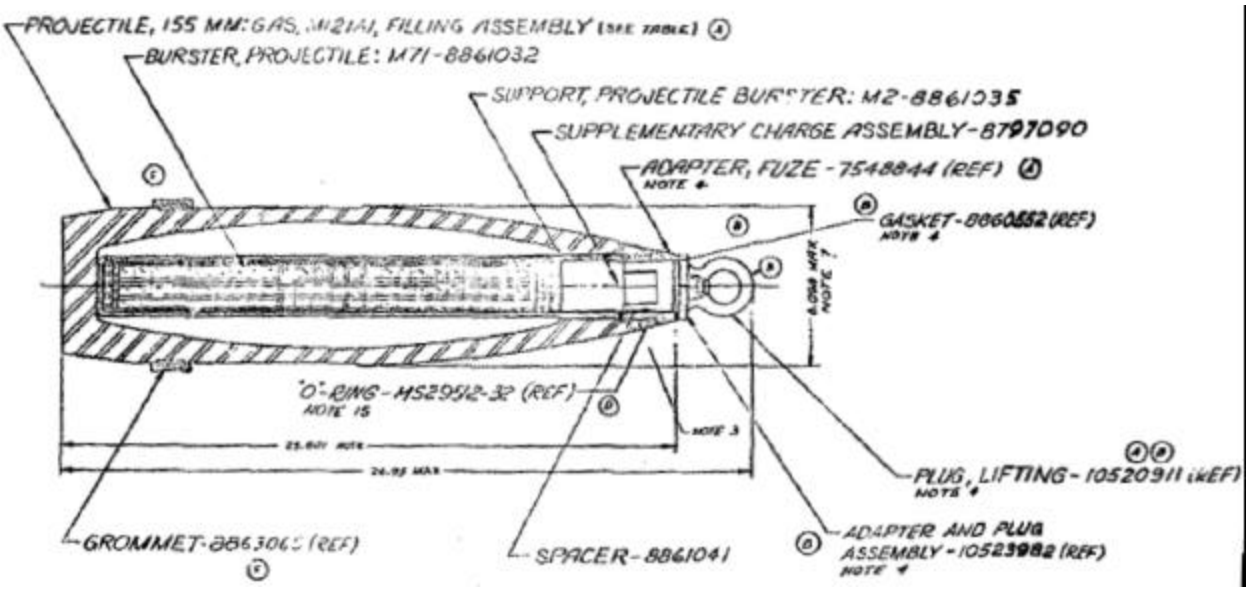

Figure 2. Drawing of the M121A1 chemical munition

The M121A1 chemical round is listed as containing approximately 2.75 lb (1.25 kg) of explosive – 2.45 lb Comp B for the main burster charge (Picatinny, 1961b), and about 0.3 lb TNT for the additional booster charge (Old Chemical Weapons Reference Guide, 1998). The munition carries approximately 6 – 6.5 lb of chemical agent (Picatinny, 1961c; Picatinny, 1961d). The munition length (without the fuze) is about 25 in, and has a listed total weight of approximately 90 - 100 lb. In the cross-section view of this projectile shown in Figure 2 (Picatinny Arsenal, 1961a), the central burster charge can be seen to extend the full length of the projectile axis. For normal function, the burster explosive would be initiated by a forward-mounted fuze and booster charge. The explosive is sheathed in a thin aluminum tube. This explosive assembly is located within a thin steel tube, centered in a base cavity that extends to the shell nose, whose purpose is to isolate the chemical agent within the munition case. The thick steel case is capped by a steel nose piece (Adapter, Fuze) that mounts the fuze or a loading ring.

The numerical model of this munition, constructed to analyze with the CTH Eulerian shock physics code, is a detailed representation of the projectile (Figure 3). A T244 fuze (MIL-HDBK, 1970) is included for the purposes of modeling a complete round. The chemical agent is normally contained in a cavity with a listed volume of 186 in^3 (Picatinny, 1961c; Picatinny, 1961d), providing a range of about 0.89 – 0.97 g/cm^3 for the agent density. In the present operational sequence, the agent has been drained from the munition, so that cavity is empty. The total mass of the model representation of the M121A1 chemical munition corresponds well to the total mass of the actual munition; the projectile production total mass may vary as much as 4.5 kg (Picatinny Arsenal, 1961a). The burster explosive, Comp B, is modeled with either a program burn option using standard JWL parameters (Dobratz and Crawford, 1985) or a reaction model option (Hertel and Kerley, 1998). The TNT booster explosive is approximated with Comp B. In the model, the total mass of the booster and burster charges is 2.96 lbs, slightly larger than the listed mass of 2.75 lb. The fuze booster explosive is modeled as PETN, also with either a program burn option or a reaction model option. The C-4 initiation explosive is modeled with a program burn option, also using standard JWL parameters (Dobratz and Crawford, 1985). The explosive model options (program burn - where the detonation is prescribed based on geometry and detonation velocity, or reaction burn – where shock amplitudes govern the initiation and detonation of the explosive) are chosen depending upon whether the fuze is operating in normal function mode (for baseline simulations) or in a destruct mode, where the fuze is initiated by the C-4 charges. For the baseline case, the PETN fuze charge is assumed to detonate (using the program burn option), and then shock-initiate the munition booster and burster charges. When the C-4 is present, it uses the program burn option, and shock-initiates all the other component explosives present in both the fuze and the munition. The material parameters for the munition and fuze are listed in Appendix A. The strain to failure for steel used in a similar munition case ranges from 15 - 30% (Picatinny Arsenal, 1962).

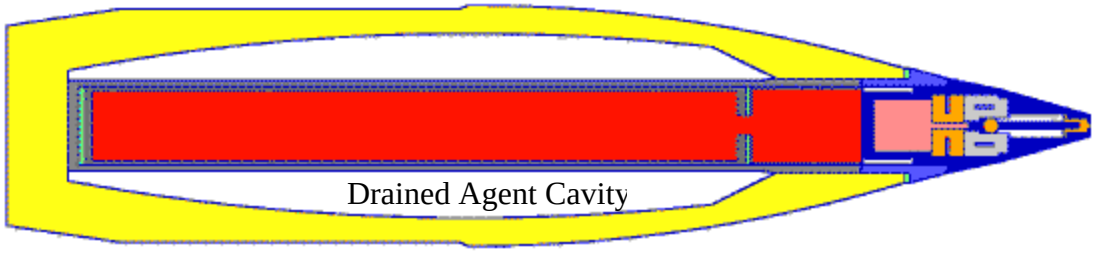

Figure 3. CTH model representation of the drained M121A1 155 mm chemical round with T244 fuze. (Munition case material is shown in yellow, burster and booster charges are red, and fuze charge is pink.) The overall length of the projectile, with the fuze present, is 69.8 cm (27.5 in).

In these analyses, all the internal components, including the fuze and burster explosive charges, are assumed to be in pristine condition. The two-dimensional baseline simulations assume that the munition case is also pristine, as shown in Figure 3. For the three-dimensional simulations, the two drain holes (0.75 inch diameter, 2.75 inch spacing) drilled into the main case body during a previous operation are included. The current analyses are focused on the effects of the additional one or two blocks of C-4 (1.25 lb/block: 1 in × 2 in × 11 in) proposed for

initiation charges. The charges are expected to be placed on the nose to ensure that the explosive charges detonate – particularly the more sensitive fuze charge. Figure 4 includes exterior views of the projectile with one (left image) or two (middle two images) blocks of C-4 attached at the nose, where the blocks are cut into 5.5 inch lengths and laid edge-to-edge (cf., Cooper, 2000). The C-4 has been formed to the curvature of the case and nose. The right hand image in Figure 4 is a cutaway view of the fuze area of the round with a one-block C-4 charge present. There are at least two options for initiating the C-4 charges – either fore or aft (towards the base of the projectile). For the single block of C-4, both fore and aft initiation options were exercised. When two blocks of C-4 were present on opposite sides of the fuze, initiation was done on both blocks simultaneously at the forward edge. In practice, this latter choice would require two detonators to be installed. When two blocks are stacked, forward detonation was assumed. An ambient air atmosphere was included in all the three-dimensional simulations.

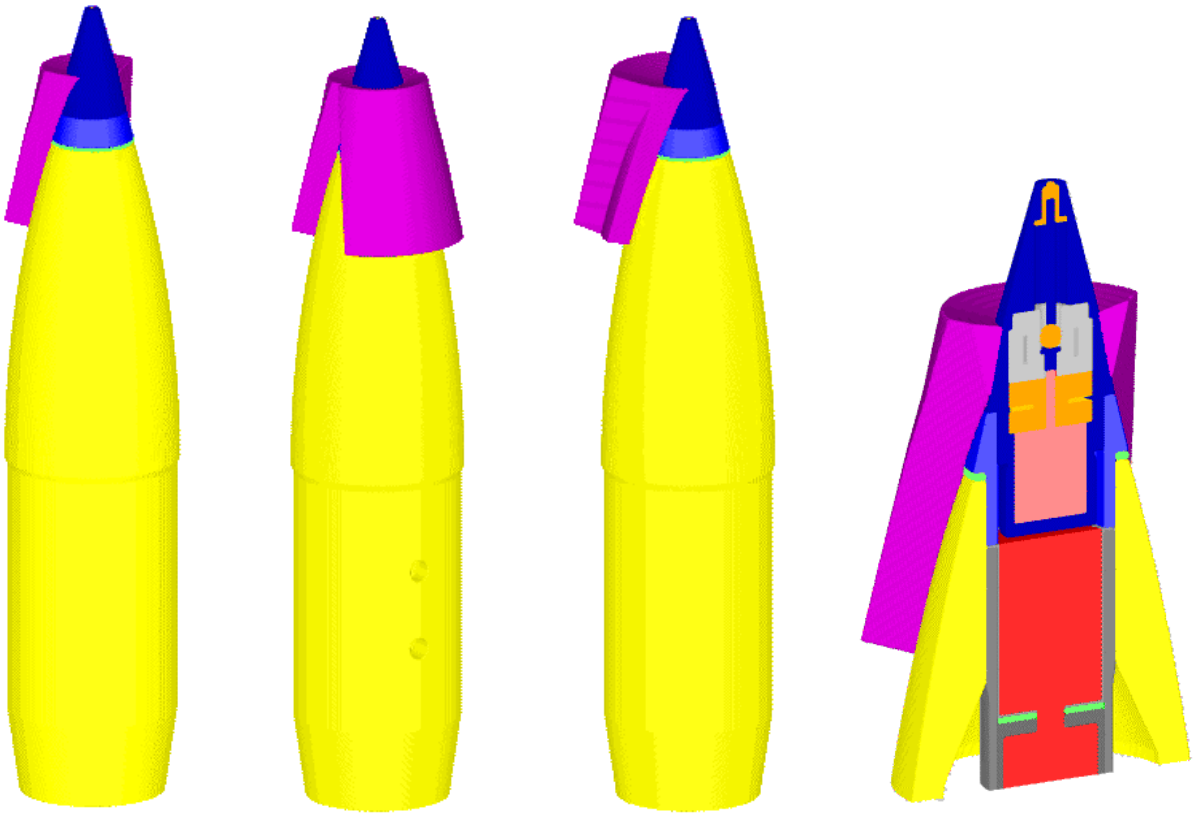

Figure 4. CTH three-dimensional model representations of the M121A1 155 mm drained chemical round with one C-4 block (left) or two C-4 blocks (opposed and stacked placement) of C-4 attached at the fuze region. A cutaway view of the fuze region with the C-4 attached is shown on the right. The drilled agent drain holes are visible in the left-center image.

Table 1 provides a breakdown of the explosive masses in the simulations by component explosive. The TNT equivalent factor for each type of explosive is noted, and the TNT equivalent of each component charge listed. The total TNT equivalent for the munition plus one and two blocks of C-4 is included.

Table 1: Explosive Component / Initiation Masses for M121A1

Explosive Component	Mass (kg / lb)	TNT Equivalent Factor	TNT Equivalent (kg / lb)
Comp B3 Burster/Booster	1.34 / 2.96	1.39	1.86 / 4.11
PETN Fuze Booster	0.06 / 0.13	1.24	0.07 / 0.16
C-4 Initiation Charge (per block)	0.57 / 1.25	1.34	0.76 / 1.68
Total TNT Equivalent (w/ 1 C-4 block)			2.69 / 5.93
Total TNT Equivalent (w/ 2 C-4 blocks)			3.45 / 7.61

To provide a perspective regarding the relative sizes of the M121A1 and the Burster Detonation Vessel, a CTH representation of them together is shown in Figure 5. Simulations combining the munition fragmentation and fragment impact onto the BDV are not feasible: after the fragments have formed at relatively small case expansions, a fully three dimensional model would be required for their diverging, free flight across the intervening space to the vessel wall. Not only is it computationally intensive to use the shock wave code to calculate the unimpeded motion of the fragments from the munition to the wall, considerable loss in fragment shape definition is lost during such a long transit through the Eulerian space.

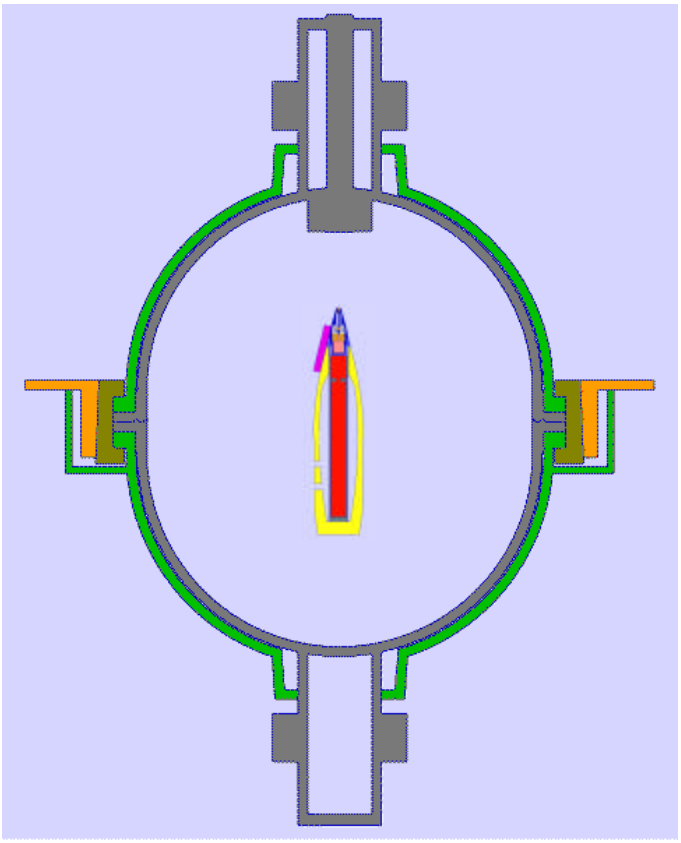

Figure 5. A view of the M121A1 located inside the Burster Detonation Vessel.

The two-dimensional simulations of the M121A1 munition could be resolved with 0.5 mm square cells, but for the three-dimensional simulations, the resolution had to be coarsened to 1 mm cubical cells. A typical three-dimensional simulation of the full munition and initiation charges present with a numerical resolution of 1 mm required 40 million computational cells. Using 1024 processors on a parallel computing platform partitions the problem so that the memory per processor is about 60 Mbytes. Approximately 70 hours of computing time are needed to calculate to a problem time of 100 μs (that is equivalent to 70,000 processor-hours of resource usage per three-dimensional simulation).

III. NUMERICAL ANALYSES OF THE M121A1 155 MM MUNITION

The initial analysis task is to determine the case fragment characteristics - dimensions and velocities - as the case expands due to the burster charge detonation after initiation by the C-4 explosive initiation charge. Extensive fragment analyses have already been accomplished for the M121A1 - without a fuze - in both full and drained conditions (Kipp and Martinez, 2000). The analyses in this section include redoing a base line simulation for the drained munition with the fuze attached, then determining whether the initiation charge leads to any deviations from the baseline fragmentation. The focus is on defining the most damaging fragments – a combination of fragment mass and associated velocity that will do the greatest damage to the BDV wall. Fragmentation of expanding cases from explosive charges have been extensively studied for fully loaded munitions (e.g., Mott, 1943; Mock and Holt, 1983), chemical munitions (e.g., Whitney, et al., 1983), and ideal cylindrical devices (e.g., Wilson, et al., 2001).

The analyses in this section focus on the drained M121A1 munition, and address the case expansion with the intent to determine fragment characteristics from both circumferential and axial breakup from the C-4 initiation and munition burster explosives. Statistics about a mean case fragment dimension are applied to estimate the largest fragment expected. Monitoring local case response to the explosive loading is accomplished with massless tracer particles attached to material at selected positions. After the fragment(s) have been characterized, consequences of impact onto the BDV are addressed in Section IV, based on results of idealized and realistic fragments that have been employed to ascertain the vulnerability of an Explosive Containment Chamber in previous studies to such incidents (Kipp, et al., 1999). Fragments will impact the Burster Detonation Vessel inner steel wall after a free flight distance of approximately 0.6 m.

The simulations of the baseline reported here are two-dimensional, and have been made with a uniform resolution of 0.5 mm. Further refinement in numerical resolution has been demonstrated to have little effect on the fracture process and fragment dimension determination, as discussed in Appendix D of Kipp, et al. (1999). The simulations of the munition with initiation charges attached are three-dimensional, with a resolution of 1 mm. With this resolution, at least 15 cells define the munition case at its thinnest regions.

A. M121A1 Drained Chemical Munition Baseline Simulations

For the baseline simulation of the drained M121A1 munition, the PETN fuze booster explosive is initiated at its forward end, as in normal function. The munition deforms as shown in Figure 6. The detonation front travels through the fuze to the main booster, and then into the burster charge. The detonation moves along the burster axis at about 8 km/s, and the reaction is complete by 76 μs. In the absence of chemical agent, the burster detonation accelerates the burster tube across the empty agent cavity to impact the inner wall of the munition case at velocities of about 1600 m/s. The thin pulse from this impact crosses the case and reflects from the outer surface of the case with sufficient amplitude to cause extensive internal fractures (spall). The ejected steel spalled material forms primarily from the outer surface of the case (Figure 6, 120 μs), and is moving at velocities ranging from 400 – 800 m/s. Maximum velocities in the fuze region are about 700 m/s.

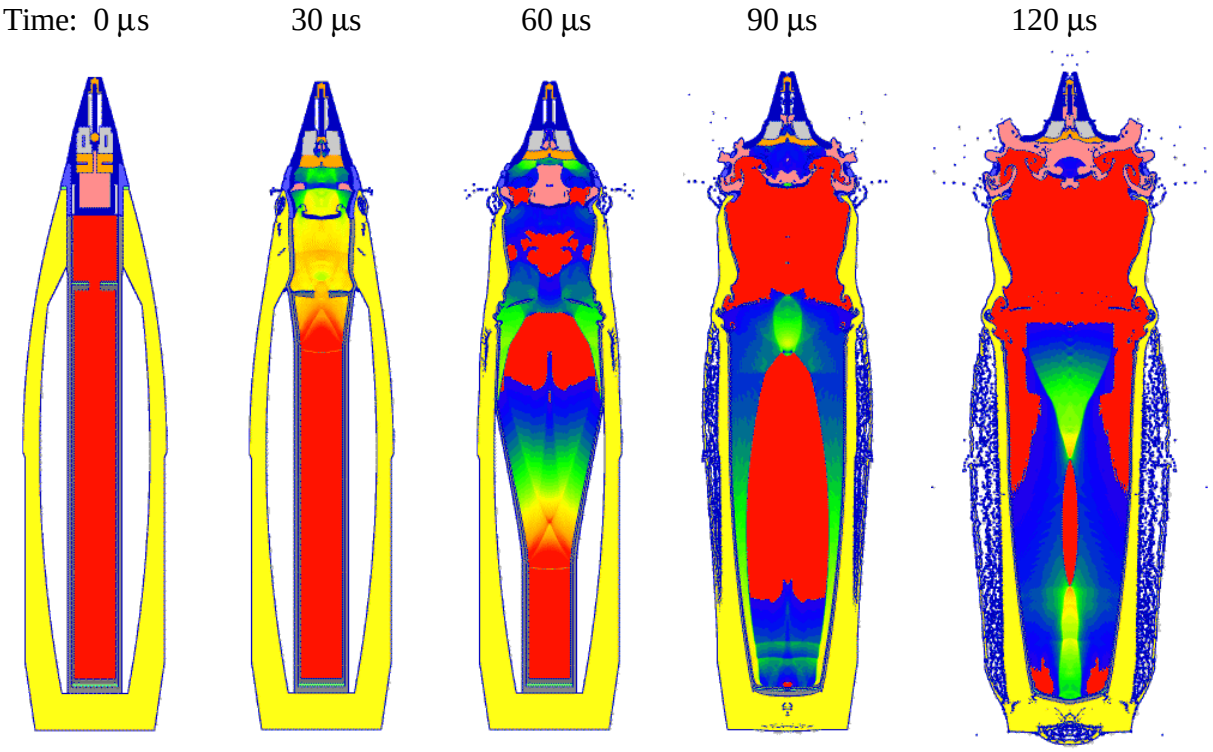

Figure 6. Simulation of normal fuze and burster charge function for the M121A1 155 mm drained chemical round. Color contours correspond to pressure amplitudes in the explosive.

These spall fragments are traveling at a much higher velocity than the bulk of the case material, which expands at about 200 – 300 m/s. This disparity in expansion velocity is reflected in the average fragment size. The slower, larger fragments are mostly of size 4 – 6 cm, which is about twice the nominal size formed when agent is present. Most of the high velocity spall fragment circumferential dimensions are approximately 1 cm or less. Detailed fragment descriptions are in Sub-section C.

The circumferential strain rate is determined from the radial expansion velocity divided by the radius. Fracture occurs sometime after 15% strain has been achieved, delayed because of lingering compression within the case created by the internal pressure of the explosive reaction products. A 15% circumferential strain corresponds to a case radius of about 9 cm. In addition to the circumferential strains, the axial strains are monitored at these tracer locations to determine when the munition will fail. The strain rates at the time of failure are used to estimate the characteristic longitudinal fragment dimensions. Axial strains in the munition were obtained by monitoring the motion of adjacent tracer positions. Typically, the axial strains were much less than 15% by the time the case has fragmented in the circumferential direction. The axial extension strain rates along the case range from 400 to 1200 /s, which correspond to fragment characteristic lengths of 20 and 9.6 cm respectively. These dimensions provide length to width ratios of at least 2. Small gradients in strain rate along the munition axis can lead to large strips, as evidenced by tests on idealized geometries, where concentric straight cylinders are used for the burster tube and case (Fischer, 1999; Stofleth, 1999). Further breakup of these fragments

would lead to shorter lengths and, as the local momentum is repartitioned, some variations about an average fragment velocity would emerge. Gradients in the expansion velocity along the fragment contribute to initial angular velocities, and rotation rates of approximately 1000 rad/s result. Typical velocities of 300 m/s give a transit time of about 2 ms to the BDV inner wall; in this interval of time, between 90 and 180 degrees of rotation are feasible.

B. M121A1 Drained Chemical Munition with C-4 Charges

When one or more blocks of C-4 are attached to the munition, three-dimensional simulations are employed to evaluate the induced motion of the projectile case and other ejected material. Views of the munition exteriors in Figure 7 illustrate the deformation associated with four variations of the C-4 charges. With one block of C-4, the charge was initiated at either its aft or forward surface (left three images in Figure 7). Deformation from two opposing blocks of C-4 and two stacked blocks of C-4 (both configurations forward initiated) are shown in the right four images in Figure 7. Note that for the two opposing blocks of C-4, ideal simultaneous initiation was presumed. In practice, typical blasting caps may have timing variations of 10's to 100's of microseconds (Stofleth, 2001). A stereo view of the forward region for one block of C-4 is included in Figure 8 to gain a perspective on the local shearing effect of the initiation charges. The C-4 initiation charge propagates a shock of sufficient amplitude and duration into the fuze and burster charges to promptly shock-initiate them, assuming they are in pristine condition.

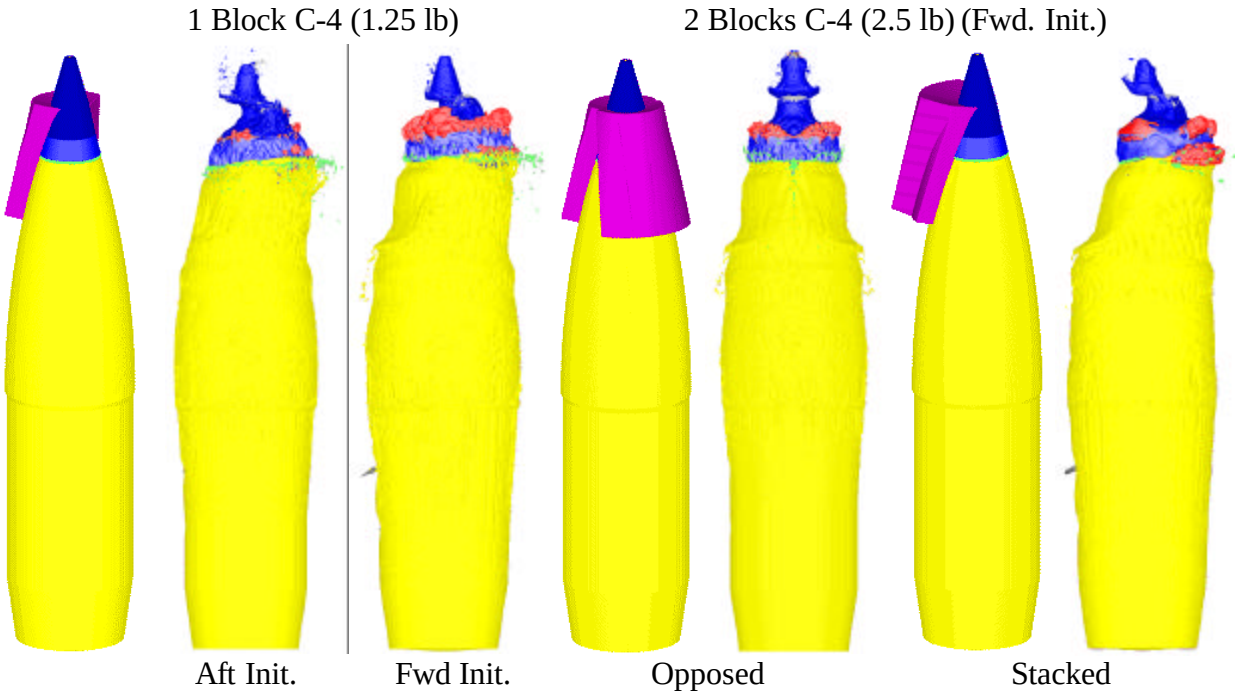

Figure 7. Exterior appearance of the munition deformation with one or two blocks of C-4. Times for the deformed images are about 100 μs. (Viewed from perspective similar to that of reference conditions shown in Figure 4.) Initiation of the C-4 charge is either on its aft-facing surface or on its forward-facing (nose) surface.

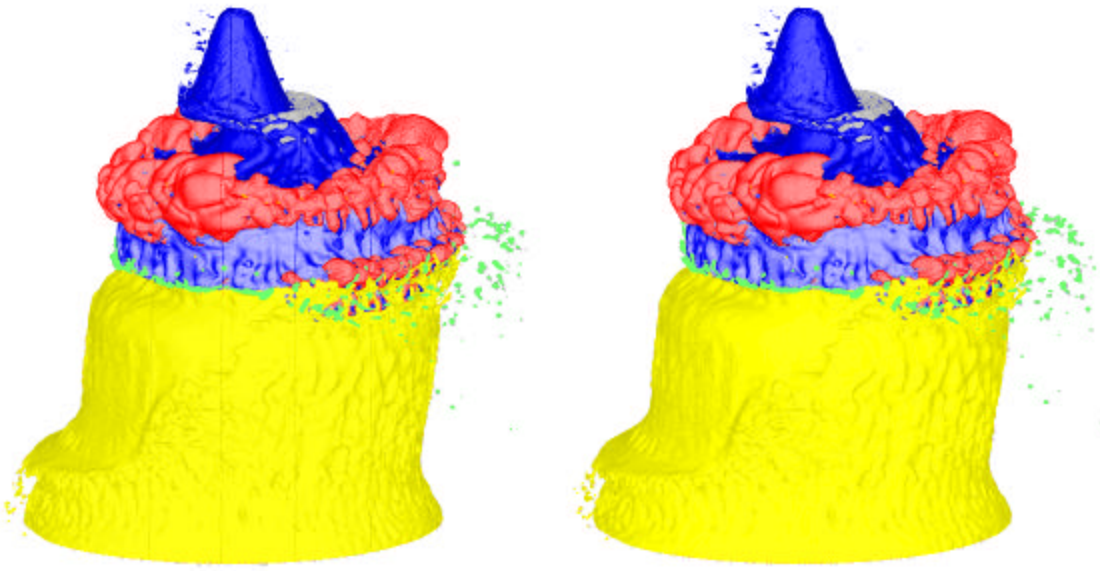

Figure 8. Stereo view of the deformed exterior appearance of the forward region of the munition with one block of C-4 (forward initiated) (100 μs) (crossed-eye view).

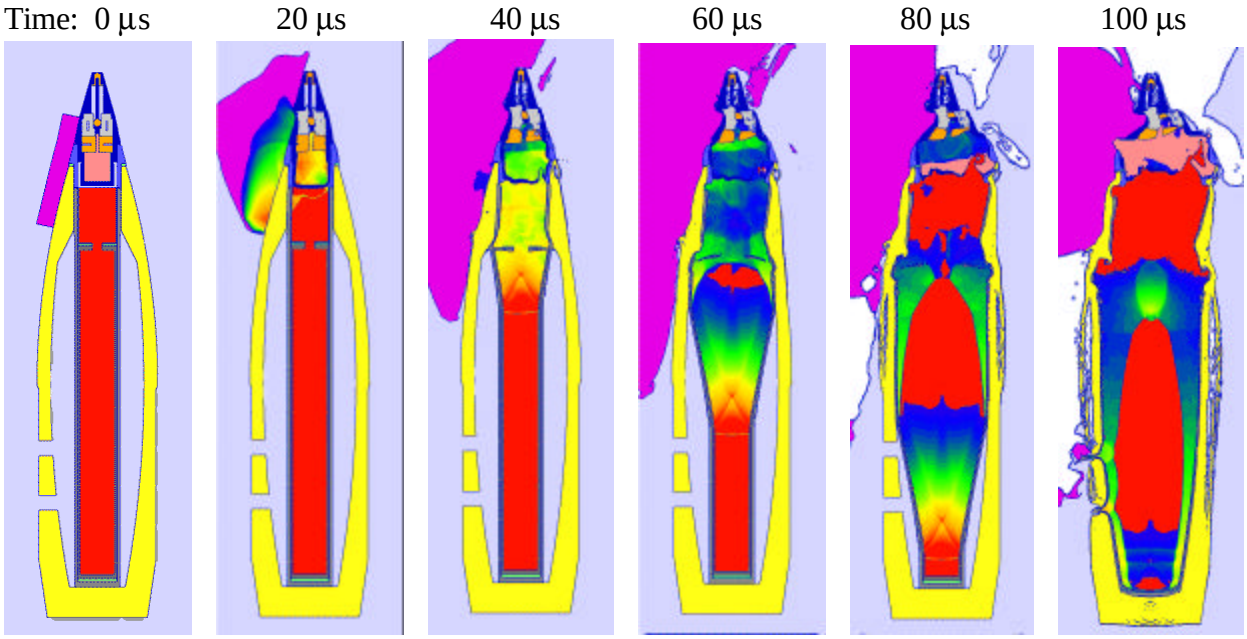

Figure 9. Simulation of one block of C-4, initiated at its forward surface, and the subsequent fuze and burster charge detonation for the M121A1 155 mm drained chemical round. Cross section through the three-dimensional geometry. Color contours correspond to pressure amplitudes in the explosive. (The gaps in the lower left munition case wall are the drain hole locations.)

A sequence of times is shown in Figure 9 for the one-block case, forward initiated, with pressure contours that define the motion of the detonation front. Although this front is clearly oblique in the fuze and booster explosives at early times (e.g., 20 μs), by 40 μs there is little evidence in the burster charge to indicate how initiation was effected. This sequence can be compared with a similar sequence in Figure 6 for the baseline normal function behavior. Since there is additional delay associated with the C-4 detonation, there is not exact time correspondence between the two sequences. However, the effect of the burster tube on the spall induced in the case is the same. The primary difference in deformation is observed in the fuze region, indicating that the C-4 effects are indeed local. Another way of evaluating this response is to look at the mid-section of the projectile at a series of times and observe that the radial expansion of the burster is quite symmetric (Figure 10). Effectively, at this axial location, the burster cannot discriminate how it was initiated.

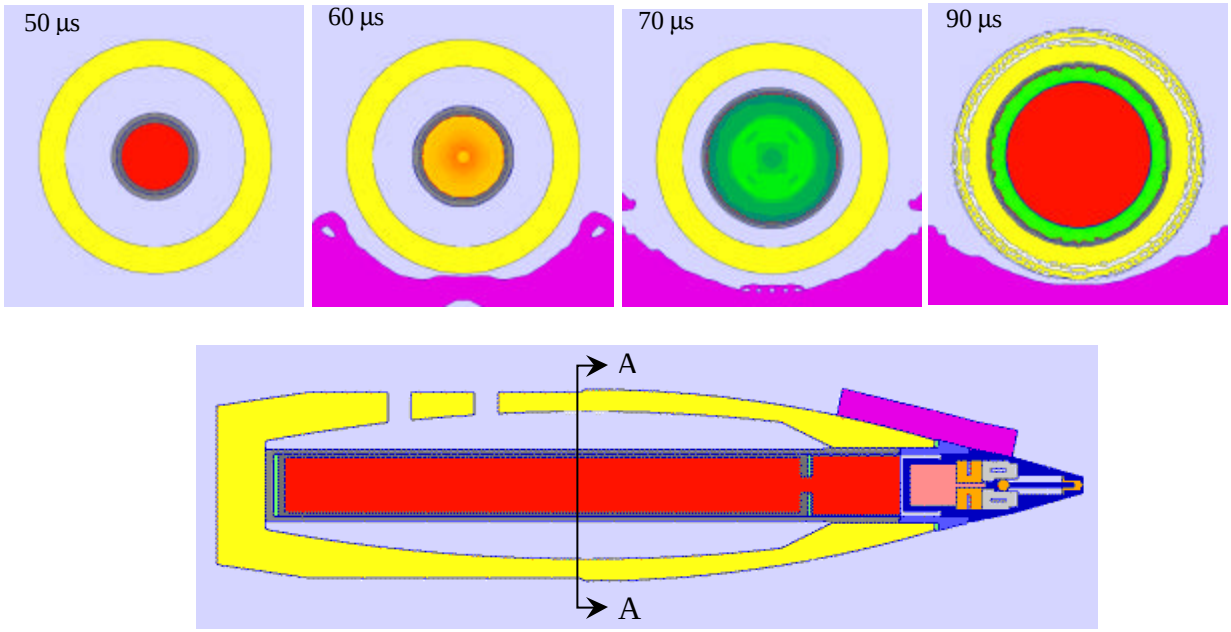

Figure 10. Cross-section of the munition with one block of C-4 (bottom). Upper views are at the mid-projectile cross-section A-A. The deformation proceeds as the detonation front passes through this location.

Case velocity comparison plots are useful to quantify the effects of the C-4 charges on the expansion velocities. In Figure 11, velocity histories in two orthogonal directions at mid-case indicate that, except for timing, the baseline and destruct configurations are quite similar. In contrast, in the fuze region (Figure 12), there is considerable difference in the case velocities, which depend on the presence or absence of C-4. Symmetric placement of two blocks of C-4 causes some case material to squirt laterally as the shocks from the opposing C-4 charges converge. Although this leads to a slightly higher velocity than the other configurations attain (Figure 12, left), the case material directly across from either a single block or two stacked blocks is also accelerated to significant velocities (Figure 12, right).

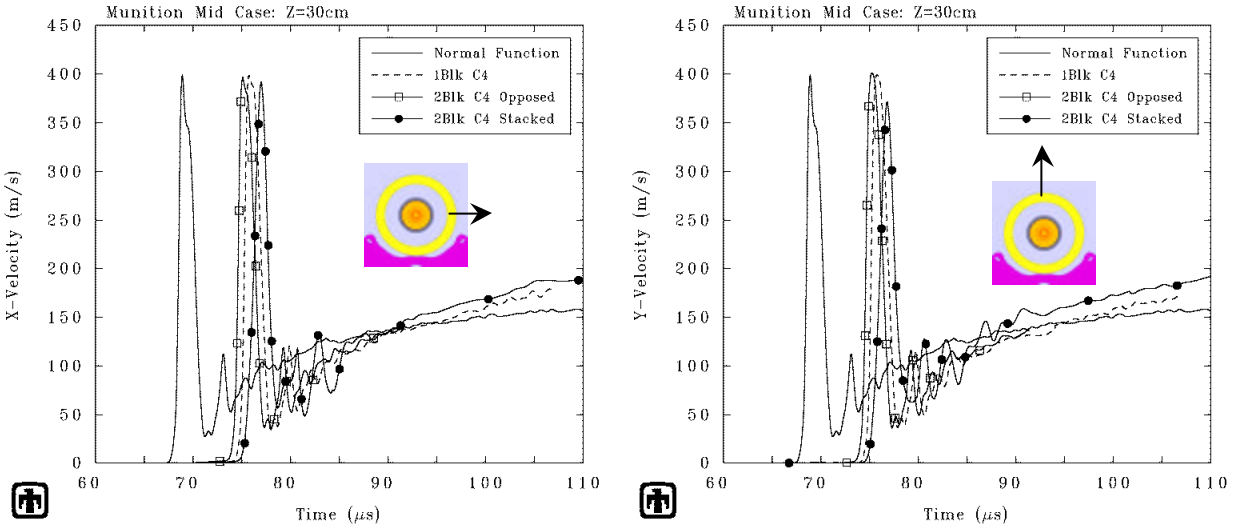

Figure 11. Expansion velocities at a mid-case location for the normal function baseline, one block of C-4, and two blocks of C-4 simulations. Velocity direction indicated on insets.

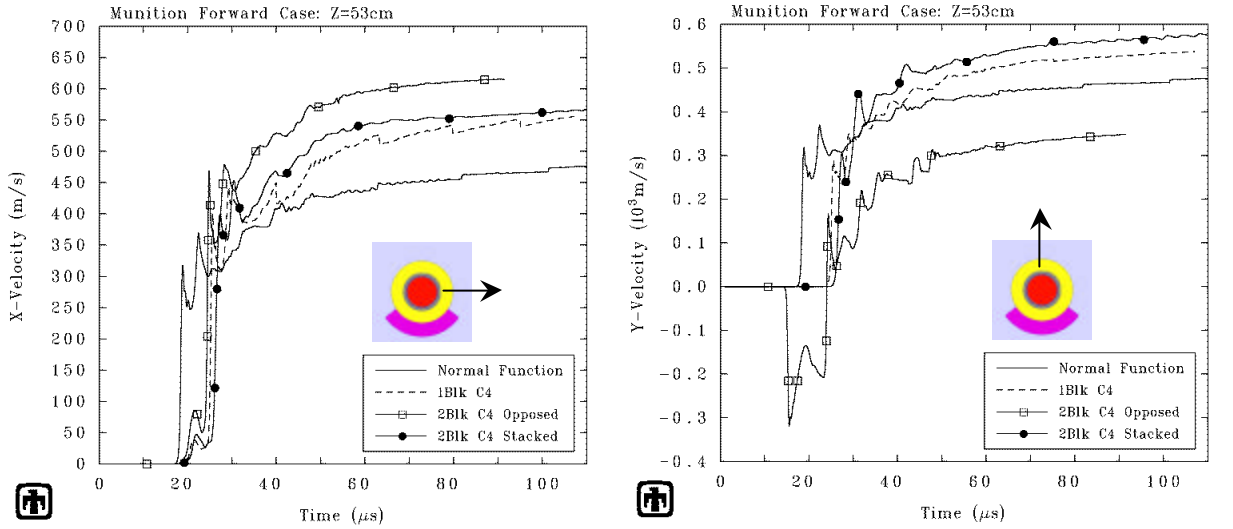

Figure 12. Expansion velocities at a forward case location in the fuze region for the normal function baseline, one block of C-4, and two blocks of C-4 simulations. Velocity direction indicated on insets.

The maximum velocities along the length of the case are plotted for each configuration in Figures 13 and 14 in two orthogonal planes. It can be seen that nearly everywhere, except in the fuze area where additional explosive has been placed, there is little to significantly distinguish the baseline from the configurations loaded with additional C-4 explosive. The slowest fragments are in the aft region of the case, and the velocity increases as the wall thickness decreases. These velocities are from the remaining thick wall of the case after the spall fragments have been ejected from the exterior.

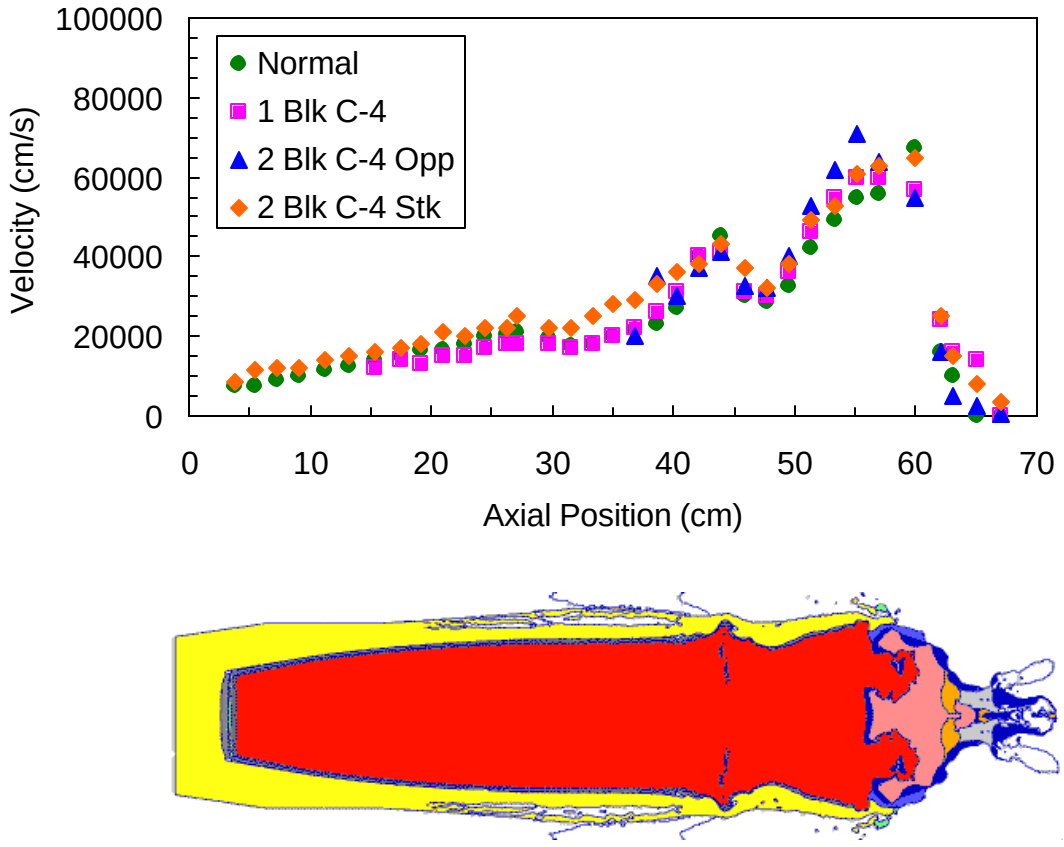

Figure 13. Maximum case expansion velocities as a function of position along the projectile for the normal function baseline, one block of C-4, and two blocks of C-4 simulations. Velocity direction is in the plane of the image.

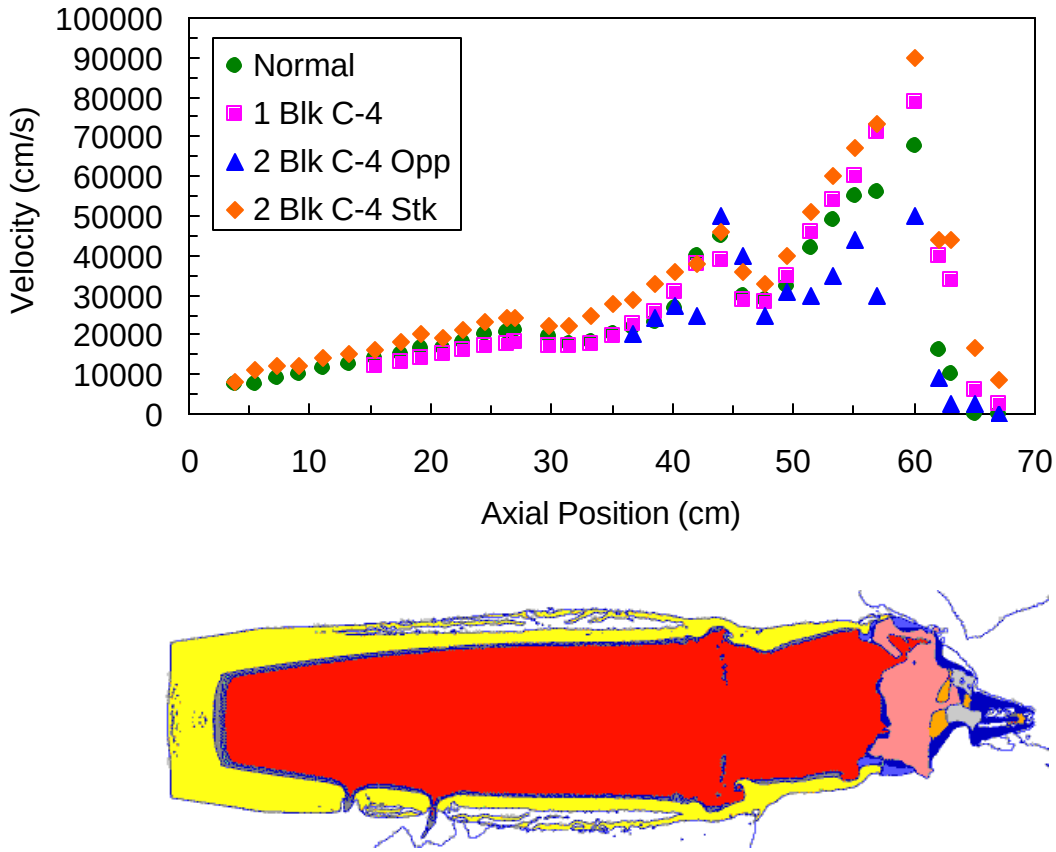

Figure 14. Maximum case expansion velocities as a function of position along the projectile for the normal function baseline, one block of C-4, and two blocks of C-4 simulations. Velocity direction is in the plane of the image (orthogonal to the plane plotted in Figure 13).

C. M121A1 Fragment Characteristics

As described in the Introduction (Section II), the local strain rate in the expanding case at the time of fracture determines the local average fragment characteristic length. This process is illustrated in Figure 15, where the strain rate history from a case location in the vicinity of the fuze is plotted. As the explosive detonates, the case expands, and the induced divergence leads to the formation of circumferential strain rates. After the strain has grown to an amplitude that corresponds to its fracture strain, the strain rate at that time is used to calculate the local average characteristic fragment dimension (based on Equation 1). From statistical techniques applied to a similar munition (Kipp, et al., 1999), the largest circumferential fragment dimension is expected to be about 40% larger than the average dimension obtained with the fragmentation model. Ratios of width to length of at least 2 were maintained to be consistent with data from certain explosive shells (Mott, 1943). The local fragment thickness is measured from the deformed munition case, including the thin (~ 2 mm) spall fragments.

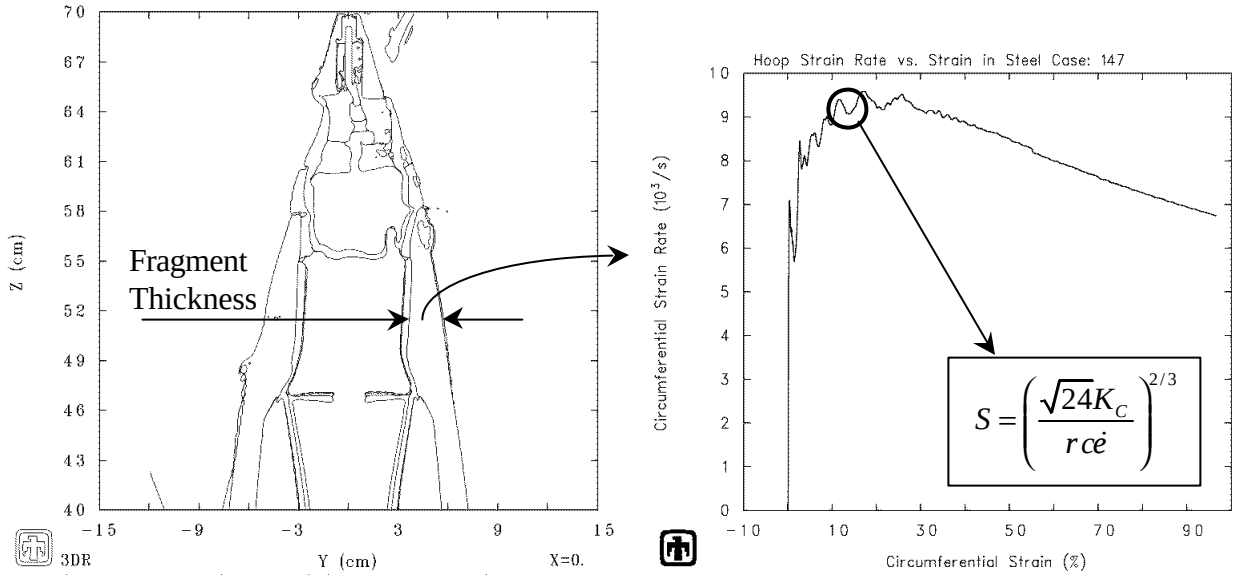

Figure 15. At a location in the munition case (left), the circumferential (hoop) strain rate can be plotted as a function of the strain (right). When the failure strain has been reached (about 15% for this material), the current strain rate is used to determine the local average fragment dimension in the circumferential direction. The case thickness provides the second fragment dimension. The axial length of the fragment is estimated from the fragment width (see text).

Figure 16 illustrates the three measures characterizing the fragment dimensions from these simulations. The right-hand image in Figure 16 is representative of how a transverse section might appear when the fracture strain has been reached. The fragment mass is obtained by factoring in the steel density. Finally, the local velocity from Figures 13 and 14 completes the characterization of a fragment. Instabilities during expansion commonly limit the lengths observed, so the narrower fragments would be expected to have shorter lengths than the wider fragments. The length is twice the width, after its 40% statistical factor increase. The fragment volume – length × width × thickness – times the density of steel (7.85 g/cm^3) provides the mass. Representative fragments determined from these numerical simulations are listed in the following tables. In these tables, the axial location is measured from the base of the munition (aft). Table 2 is reprinted from Kipp and Martinez (2000) for one of the drained munition scenarios reported in that reference in which no initiating charge was present. Table 3 includes fragments selected from the three-dimensional simulation of one-block of C-4, and Table 4 includes fragments from a munition initiated with two stacked blocks of C-4. Since there is minimal difference in the aft section of the projectile between the baseline and the destruct configurations, the focus of both Tables 3 and 4 is on fragments formed in the forward (nose) section of the projectile. In some fuze locations, the calculated fragment dimension is larger than the component itself, and the table reflects some adjustments made to accommodate these physical size constraints. In these tables, only the fragment width (column 3) is directly calculated with Equation 1 using the local strain rate. Note that these fragment widths in Table 2

were calculated using an average value of fracture toughness, 180 MPa $\sqrt{m}$ (Kipp and Martinez, 2000), and the fragment widths in Tables 3 and 4 for the current analysis were made with the upper limit value of 265 MPa $\sqrt{m}$ for the fracture toughness. This modification in fracture toughness was made to provide upper bounds on the expected fragment dimensions. The effects will be clearly seen in the vulnerability plots in the next section. Based upon the way the fragment dimensions are being defined in these tables, the width effectively enters as a factor twice – once as the width (times 1.4), then again in the length, which is twice the width. From Equation 1, this means that the mass is affected by the fracture toughness to the 4/3rd power. Hence, an increase from 180 to 265 MPa $\sqrt{m}$ for the fracture toughness increases the mass by a factor of about 1.7 for the same strain rate.

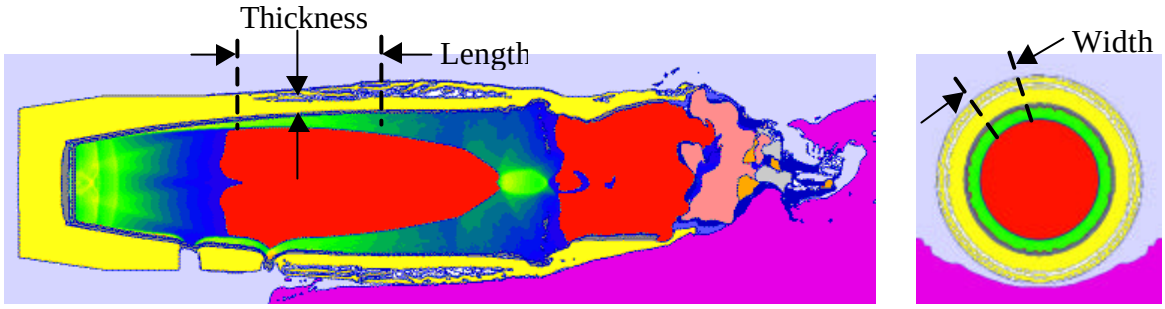

Figure 16. Characteristic fragment dimensions.

Table 2: M121A1 Fragment Masses and Velocities (Aft Initiation, 0% Agent, Without a C-4 Initiating Charge) (from Kipp and Martinez, 2000)

Axial Position (cm)	Thickness (cm)	Width (cm)	Width × 1.4 (cm)	Length (Width × 2) (cm)	Fragment Mass (g)	Fragment Velocity (m/s)
11	0.9	3.4	4.8	9.5	320	225
16	0.27	1.4	2.0	3.9	16	340
23	0.18	0.7	1.0	2.0	2.7	325
31	0.15	0.55	0.8	1.5	1.4	650
38	0.1	1.5	2.1	4.2	7.0	785
43	0.1	0.55	0.8	1.5	0.9	840
5	2.7	6.0	8.4	16.8	2991	80
11	1.5	5.6	7.8	15.7	1409	170
16	1.4	5.3	7.4	14.8	1167	200
23	1.1	5.1	7.1	14.3	872	200
31	1.2	6.1	8.5	17.1	1363	150
38	1.1	5.9	8.3	16.5	1168	150
43	0.9	4.6	6.4	12.9	586	205
50	1.8	3.5	4.9	9.8	686	290

Note: First six rows are spall fragments.

Table 3: M121A1 Fragment Masses and Velocities (1 Block C-4, 0% Agent)

Axial Position (cm)	Thickness (cm)	Width (cm)	Width × 1.4 (cm)	Length (Width × 2) (cm)	Fragment Mass (g)	Fragment Velocity (m/s)
40.25	0.95	4.3	6.02	12.04	541	310
42.11	1.9	3.7	5.18	10.36	800	380
43.97	1.6	3.5	4.9	9.8	603	390
45.83	0.8	3.9	5.46	10.92	374	290
47.69	1.6	4.1	5.74	11.48	828	285
49.56	1.6	3.5	4.9	9.8	603	350
51.42	1.4	2.9	4.06	8.12	362	460
53.28	1.1	2.5	3.5	7.0	212	540
55.14	0.8	2.3	3.22	6.44	130	600
57	0.5	2.2	3.08	3*	36	710
60	0.5	2.1	2.94	3*	35	790
62	0.8	2.2	3.08	4*	77	400
63	0.3	2.5	3.5	3*	25	340
64	0.3	4.7	6.58	3*	46	60

* Component size limits imposed on fragment dimensions

Table 4: M121A1 Fragment Masses and Velocities (2 Stacked Blocks C-4, 0% Agent)

Axial Position (cm)	Thickness (cm)	Width (cm)	Width × 1.4 (cm)	Length (Width × 2) (cm)	Fragment Mass (g)	Fragment Velocity (m/s)
40.25	0.95	3.9	5.46	10.92	445	360
42.11	1.9	3.7	5.18	10.36	800	380
43.97	1.6	3.5	4.90	9.8	603	460
45.83	0.8	3.9	5.46	10.92	374	360
47.69	1.6	3.8	5.32	10.64	711	330
49.56	1.6	3.3	4.62	9.24	536	400
51.42	1.4	2.6	3.64	7.28	291	510
53.28	1.1	2.3	3.22	6.44	179	600
55.14	0.8	2.2	3.08	6.16	119	670
57	0.5	2.2	3.08	3*	36	730
60	0.5	1.9	2.66	3*	31	900
62	0.8	2.3	3.22	4*	81	440
63	0.3	2.3	3.22	3*	23	440
64	0.3	3.2	4.48	3*	32	165

* Component size limits imposed on fragment dimensions

IV. FRAGMENT IMPACT CONSEQUENCES ON THE BDV

It should first be noted that with a minimum yield strength of 620 MPa, the steel Burster Detonation Vessel wall is susceptible to local permanent deformation from any steel fragment with an impact velocity in excess of 50 m/s. For steel impacting steel, the shock jump conditions relate the impact stress, s, to the density, r, shock velocity, U_s, and impact velocity, V_{IMP}, as

$$s = r \cdot U_S \cdot \frac{V_{IMP}}{2} \quad . \tag{2}$$

At low impact velocities, the shock velocity is approximated by the longitudinal velocity, about 5000 m/s for steel; the density of steel is 7800 kg/m^3, and the stress to reach yield, the Hugoniot Elastic Limit, s_{HEL}, is related to the yield stress, Y_0, through the Poisson's ratio, n (0.28 for steel),

$$s_{HEL} = Y_0 \cdot \frac{1-n}{1-2n} \tag{3}$$

From these relationships and material properties for the steel, the threshold velocity for the impact stress to equal the Hugoniot elastic limit stress is determined to be about 50 m/s. Figures 13 and 14 indicate that the fragment velocities from the exploding M121A1 munition range from about 100 to 900 m/s. Clearly, all these fragments have sufficient velocities to cause some local deformation when impacting the BDV walls. What must be determined is the extent of the deformation, and whether the BDV wall is vulnerable to perforation by any of these fragments.

The shock stress amplitude defined by Equation 2 can also be used to estimate the impact velocity required to spall the target when flat impact of a fragment occurs. The transmitted compressive pulse, under ideal flat plate impact conditions, essentially unloads into a state of tension internal to the target of amplitude equal to the compressive pulse magnitude. With a spall stress of about 4 GPa for steel, an impact velocity of 200 m/s is sufficient to generate such tensile stresses for incipient spall conditions. Fragment impacts are not ideal, however, with irregular fragment geometry, curved surfaces, and non-planar impact, so velocities in excess of this threshold are expected to be required to effect spall.

In a previous study of a comparable munition (M426, 8 inch, chemical) two approaches to fragment impacts onto an Explosive Containment Chamber (ECC) wall (30 mm) were taken to determine a ballistic limit velocity/mass curve (Kipp, et al., 1999): (1) three-dimensional analyses of fragment impacts, and (2) two-dimensional idealizations of those fragments as long cylindrical rods. The first method captures some aspects characteristic of fragment impact, including some irregularities associated with explosively formed fragments, but only limited parameter variations can be addressed in such three-dimensional analyses. An alternative was to transform the cross-sectional area of the original fragments into a circular section of equivalent area, so long-rod axi-symmetric simulations could be employed to examine fragment impact onto the ECC. Variations of such idealized fragments were readily made. In order to place the simulations into an experimental context, one long-rod impact case was used as a benchmark to check the code accuracy in this limit velocity application (Appendix C in Kipp, et al., 1999). Those CTH simulations were found to underestimate the ballistic limit velocity by about 15%.

Hence, the CTH numerical simulations are conservative in their prediction of perforation, tending to indicate somewhat more damaging effects than actually occur. In those analyses, the model for the steel assumed a yield strength of 480 MPa, which is somewhat smaller than the minimum yield strength of 620 MPa that characterizes the Burster Detonation Vessel (Hilding and Nilsson, 2001). At least as important is that the analyses were based on a 30 mm wall thickness, whereas the current wall thickness has been increased to 40 mm.

The limit velocity curves plotted in Figure 17 for the 30mm ECC wall are based on both CTH simulations and the empirical limit velocity expression described in Appendix C of Kipp, et al. (1999). As noted above, for a single example, CTH tends to calculate a penetration at a given velocity that is too large by about 15%. The limit velocities are larger than the CTH calculations at all impact conditions, consistent with the under-prediction of limit velocity by CTH in the normalization example. It should be noted that the coefficient for the empirical curve is based on a projectile yield strength about twice that of the M121A1 case material, and a target yield strength comparable to that of the Burster Detonation Vessel wall. As described earlier, the large radius of the chamber provides ample time for fragments from a source near the center of the chamber to rotate in flight. Normal, end-on impacts on a local region of this wall are expected to be the most damaging orientation. Side-on impact by heavy fragments was shown to cause extensive local deformation, but no perforation.

The M121A1 fragment characteristics from the previous tables (Tables 2, 3, and 4) are plotted in Figure 17. In all cases for this drained munition, the fragments appear to be within safe limits of incidence on the Burster Detonation Vessel inner wall. Note that the points from Tables 3 and 4 (the three-dimensional cases, with one and two blocks of C-4) are clearly shifted relative to the points from the previous analyses. As noted in the previous section, the new points were calculated with a larger value of the fracture toughness than the previous values, hence leading to larger fragment width estimates. The new points are effectively shifted to the right on this plot by a factor of 1.7 compared to the former points. Reducing the masses of the new points by 1.7 would bring all the points into a fairly common envelope relative to the limit curves. However, the larger value of fracture toughness was used specifically to emphasize the effect that material parameter has on the fragment mass, and the consequences for vulnerability analysis.

A limited amount of arena test data on the fragmentation of the M122 munition (which appears to be a virtual copy of the M121A1 considered here) containing agent is reported in Whitney, et al. (1983), drawn from another report (Dugway, 1974). The measured fragment masses and velocities (Table 5) are keyed to the sections of the munition as illustrated in Figure 18. These data include both average mass and largest mass fragments. The fragments from simulations referenced in Table 2 are the largest expected from a drained munition, in which significantly more spall fragments form than when agent is present. A better comparison can be made with fragments determined from previous simulations (Kipp and Martinez, 2000) for a filled munition (Table B1 in that report). There, the largest mass corresponding to Regions A/B was about 500 g with a velocity of 350 m/s; the largest mass corresponding to Regions C/D was about 400 g, with a velocity of 425 m/s. A detailed comparison with the fragment sizes calculated from the numerical simulations requires a more complete description of the raw fragment mass and velocity data, and a simulation of the exact device used in the data arena test.

A limit velocity curve for the 40 mm wall (from Table B1, Appendix B) and fragment points are replotted in Figure 19, augmented by the M122 data from Table 5 and estimated fragment sizes for the Livens, 4.2 inch mortar, Stokes Mortar, and 75 mm Mk II munitions from Table C2. All the calculated points from the drained M121A1 munition that were in Figure 17 are now plotted as a single family of open circles. All the fragments are now considerably removed from this limit velocity curve. For the munitions with less explosive mass, there appears to generally be a large margin of safety, and all of the M122 data points (both average and largest fragment) fall within the scatter of the calculated points, with none exceeding the limit curve. The velocities from all the fragments, however, are still above the cratering threshold of the inner steel wall. As was discussed in constructing the characteristic fragment dimensions for the tables, in many cases a length of twice the statistical width was employed. From the plot in Figure 19, it is apparent that were the lengths of these uniform cylindrical shells to be 4 – 5 times the width (about doubling the fragment mass), the resulting shift in the fragment positions by such a factor to the right would still not intersect the limit velocity curves (for a 40 mm chamber wall).

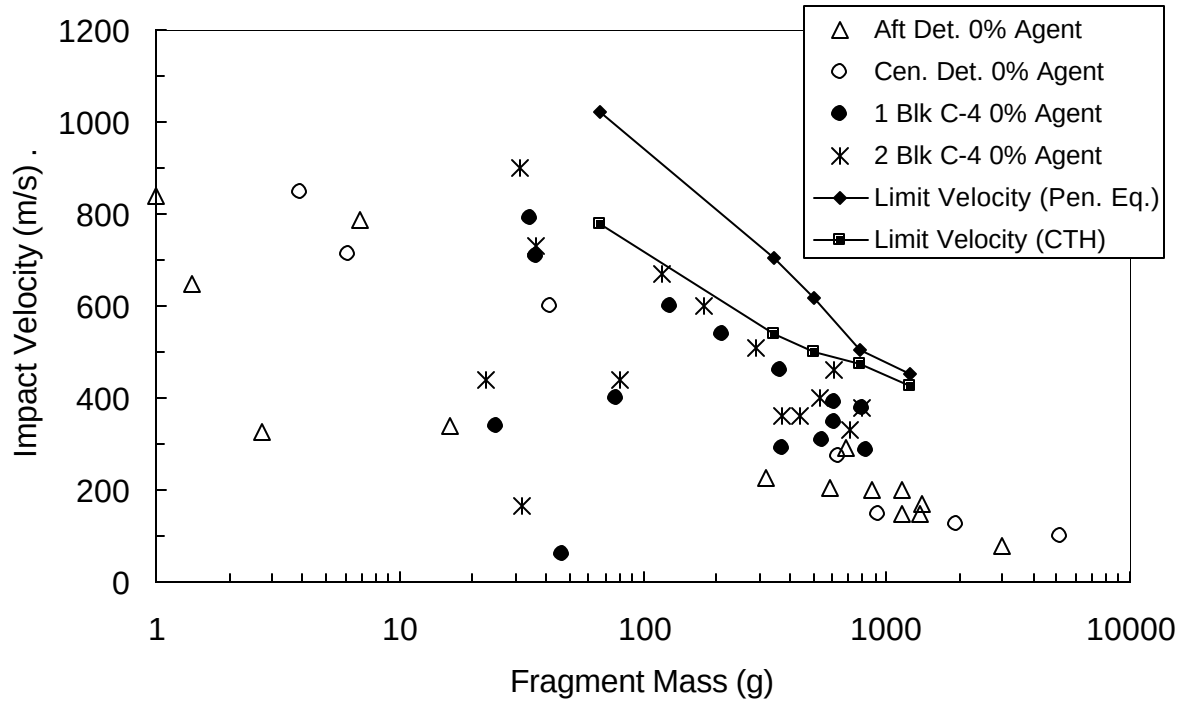

Figure 17. Limit velocity curves for fragment impact on a 30mm steel wall, with representative fragments from the numerical simulations of the M121A1 chemical munition. "Aft Det. 0% Agent" and "Cen. Det. 0% Agent" points are extracted from Kipp and Martinez (2000) for the M121A1 without a fuze or any C-4 charges present. "1 Blk C-4 0% Agent" points are from the analyses in this report. Limit velocity curves also from Kipp and Martinez (2000).

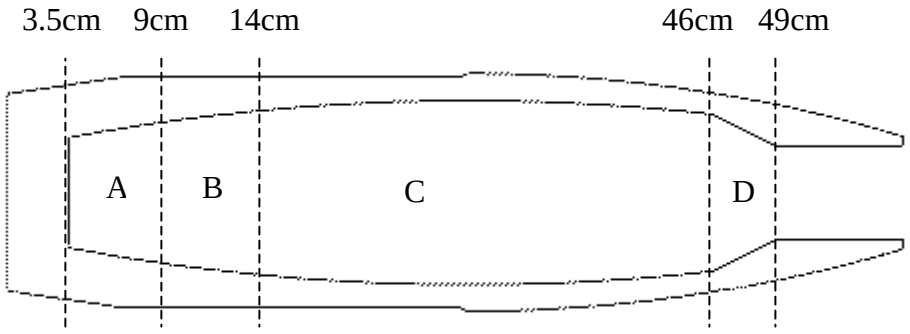

Figure 18. Source key for the M122 case fragment data collection regions (Whitney, et al., 1983). The axial locations of the region boundaries, measured from the base of the projectile, are indicated above the sketch.

Table 5: M122 Fragment Mass and Velocity Arena Test Data (with Agent) (from Whitney, et al., 1983)

Region	Average Velocity (ft/s / m/s)	Average Mass (lb / g)	Largest Mass (lb / g)	Velocity Associated with Largest Mass (ft/s / m/s)
A	1047 / 320	0.042 / 19	2.30 / 1040	1200 / 365
B				
C	1328 / 405	0.010 / 4.5	0.26 / 118	1750 / 535
D				
Base	750 / 230	0.846 / 384	4.80 / 2200	750 / 230

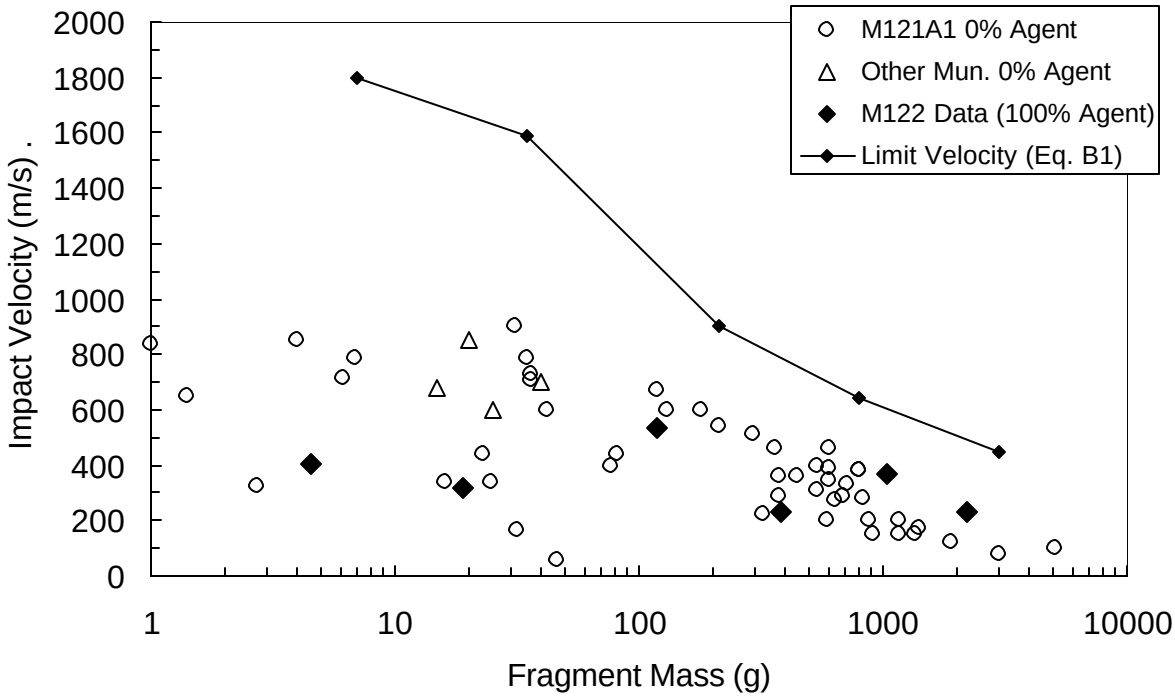

Figure 19. Limit velocity curve for fragment impact on a 40mm steel wall, from Appendix B. Representative fragments are from the numerical simulations of the drained M121A1 chemical munition (Tables 2, 3 and 4), the four munitions summarized in Appendix C (Table C2), and the data from Table 5 for an undrained M122.

V. DISCUSSION OF RESULTS

The analyses of the drained M121A1 chemical munition with C-4 initiation charges made for this study indicate that the steel chamber will not be perforated by any of the fragments from the deliberate detonation of the munition burster charge. Damaging penetrations, however, may need remediation so later strikes cannot perforate the inner wall. (The fragment field is diverging, so multiple large fragment strikes at the same position are not likely in any single event). Large fragments (mass > 100 g) with velocities of 100 to 700 m/s can be expected from this round, velocities at which substantial local permanent deformation will occur at the impact sites. The fragments formed at the base end of the M121A1 munition, where the case has its greatest thickness, are expected to cause the most local deformation of the inner wall, but less massive, faster fragments penetrate to larger depths. This region of the munition is unaffected by the presence of the initiation charge, which contributes only locally (the nose region) to fragment velocities and dimensions. In the M121A1, there is only modest change to the fragment formation due to the addition of the initiation charge when compared to the baseline normal function configuration. The largest increase in local velocity occurs in a scenario where two C-4 blocks are placed on top of each other on the same side of the munition rather than in an opposed placement. Despite this increased local velocity, the fragments from this region are small (Tables 3 and 4), and the limit velocity plot in Figure 19 indicates a large margin between these fragments and the limit velocity curve for all fragments with mass smaller than 100 g.

In the current scenario where the agent is absent, the burster explosive products undergo some initial expansion prior to engaging the munition case, resulting in less efficient acceleration of the case, and lower terminal velocities for the large fragments than when agent is present. In this absence of agent, the explosive accelerates the thin burster tube in free expansion, possibly fragmenting it during transit to the munition case. When these fragments with very high fragment velocities impact the case, exterior spall fragments are formed. Although these ejected fragments typically have the highest velocities of any of the case fragments, they have the least associated mass, and fall well within the limit velocity curve.

This study has identified large fragment masses from the munition case as the most damaging objects formed in the detonation of the burster and initiation charges. The strain rate magnitudes govern the average munition fragment dimensions as the case expands, and statistical measures were applied to these averages to arrive at the characteristic dimensions of the largest expected fragment. (e.g., The factor of 1.4 is used as a reasonable measure of largest fragment size relative to the average calculated dimension.) The limited amount of arena test data made available here confirm that the calculated fragment sizes are reasonable estimates of what could form from this event. If raw fragment data become available, a better judgement on the veracity of the simulations in this application can be made. As noted in the report, comparisons of the model to data from more idealized cylinders has shown that not only are the average sizes quite well described, experimental and simulated size distributions also agree very well (Wilson, et al., 2001). As is clear in the expression for the average fragment size (Equation 1), the fracture toughness is a critical material property. Variations in this parameter contribute directly (at $2/3^{rd}$ power) to the fragment width. Uncertainties in this parameter, as illustrated in the fragment points plotted in Figure 17 using two different values for the fracture toughness, do not lead to fragments exceeding the limit velocity curve.

In a previous analysis of the effects of a pre-cracked munition case on fragment size (Kipp and Martinez, 2000, Appendix D), it was demonstrated with one example that no significant increase in average size will occur relative to the natural average fragment size already defined by the existing munition case velocities. The strain relief propagated from the site of the pre-crack during case expansion does not have enough time to exert much influence on the dominant natural fragmentation. These pre-existing flaws (gouges, pitting, cracks, etc.), despite being preferential failure locations, do not lead to unusually large fragments (e.g., splitting the munition case into a few large sections). Such flaws provide only a minor increase in the natural average fragment size adjacent to the flaw site. The large strain rates associated with the high divergent expansion velocities fundamentally preclude the formation of fragments encompassing large angular sections of the case.

In the cases of other munitions whose drained fragmentation conditions were summarized in Appendix C, there are still additional analyses that could be made to do a more complete mapping of the fragment formation. Although the fragment masses and velocities in Table C2 are representative, they were extracted from only the primary cross-section of the munition. No analyses were made with the addition of the C-4 initiation charges, so the additional velocity component in the vicinity of those charges is not accounted for. Based on the burster charge masses in Table C1, one C-4 explosive block exceeds the explosive mass in all the munitions except the M121A1. Determining the response when C-4 in contact with the less massive construction of those munitions is a task that could be undertaken to verify that no unusually damaging fragments are formed.

Limited comparisons of numerical simulations with Gurney velocity and independent penetration data in the previous study of the M426 munition indicated that the code provides accurate measures of the expansion velocities, but tends to overpredict the extent of penetration at a given impact velocity. In addition, recent tests have been done by Fischer (1999) and Stofleth (1999) of scaled chemical munitions with central burster charges to examine the case breakup characteristics. Steel witness plates placed near the device have consistently indicated less cratering damage than expected based simply on the yield strength being exceeded. This has suggested that there are some profitable studies to be made that would quantify the damage levels caused by the fragments from these rounds. Consequently, the results reported here are considered worst-case evaluations of the vulnerability of the Burster Detonation Vessel to munition detonation.

VI. CONCLUSIONS

The primary result from this study of the drained M121A1 chemical munition with C-4 initiation charges is that the Burster Detonation Vessel chamber walls will not be perforated by any of the fragments formed by the deliberate detonation of the munition fuze and burster charges. The following conclusions may be drawn from the current analyses of the drained M121A1 munition using both the CTH Eulerian shock physics code and analytic techniques:

- The Burster Detonation Vessel has two 40 mm thick walls of cast stainless steel, S165M, and a single detonation event with initiation charges is extremely unlikely to perforate the inner wall, let alone the outer wall.

- Analytic considerations of fragment impacts indicate that above a threshold velocity of about 50 m/s, some local deformation to the BDV walls is possible, independent of thickness. Virtually all the fragments exceed this impact velocity, so some damage to the interior exposed surface of the vessel must be expected.

- There is the additional possibility of internal spall damage, under ideal impact conditions (i.e., flat, plate-like normal impact), when impact velocities exceed 200 m/s. Again, many fragments have significantly higher velocities than this, and some consideration should be given to assessing such damage.

- Under ideal conditions, a single block (1.25 lbs) of C-4 applied to the munition nose region appears to be adequate to initiate both the fuze and burster charges. No account was made of possible sensitivity effects associated with aging of the explosive components (e.g., the burster charge may be approximately 40 years old).

- If two initiation blocks of C-4 are present in a configuration that would require simultaneous initiation (as in the arrangement where the blocks are on opposite sides of the nose), the timing variation of the blasting caps is sufficiently large (10's to 100's of microseconds) that some means should be made to ensure simultaneity of initiation.

- The burster charge is the primary energy source for munition case fragments. The presence of the C-4 initiation charges primarily affects the mass and velocity characteristics of the fragments in the immediate region of the charge, and has little influence elsewhere.

- Relative to normal function of the munition (fuze and burster), the maximum local increase in velocity of fragments near the C-4 initiation charge is about 50%.

- The calculated fragment masses and velocities for the M121A1 appear to be similar to the limited fragment information available from arena test data on similar munitions.

VII. REFERENCES

ConWep computer code, U.S. Army Corps of Engineers (May 1989). Based on "Fundamentals of Protective Design for Conventional Weapons", TM 5-855-1, November 1986.

Cooper, P. W. (2000). "Initiation of Various Drained Munnitions", Memo, February 20, 2000.

Dobratz, B. M. and P. C. Crawford (1985). "LLNL Explosives Handbook. Properties of Chemical Explosives and Explosive Simulants", Lawrence Livermore National Laboratory Report, UCRL- 52997, Change 2, January 1985.

Dugway (1974). "Support Test for Evaluation of a Suppressive Shield – Containment Facility for Chemical Agent Munition Disposal System", Dugway Proving Ground, Dugway, Utah, 84022, April 1974.

Dynasafe (2000). Dynasafe Design Drawing 000312-1/C, September 29, 2000.

Fischer, S. H. (1999). Sandia National Laboratories, Personal Communication.

Grady, D. E. (1988). "The Spall Strength of Condensed Matter", J. Mech. Phys. Solids, 36, 353-384.

Group GMX-6 (1969). "Selected Hugoniots", Los Alamos Scientific Laboratory Report LA-4167-MS.

Hertel, E. S., Jr. and G. I. Kerley (1998). "CTH Reference Manual: The Equation of State Package", Sandia National Laboratories Report SAND98-0947, April 1998.

Hilding, D. and L. Nilsson (2001). "Simulation of Dynamic Tests for DYNA PROJ 137", Engineering Research AB Report ERAB-01:15, Ver. 1, 2001-09-07.

Jones, G. E., J. E. Kennedy, and L. D. Bertholf (1980). "Ballistics Calculations of R. W. Gurney", Am. J. Phys., 48, 264-269.

Kennedy, J. E. (1970). "Gurney Energy of Explosives: Estimation of the Velocity and Impulse Imparted to Driven Metal", Sandia Laboratories Report SC-RR-70-790, December 1970.

Kipp, M. E., D. E. Grady, and J. W. Swegle (1993). "Experimental and Numerical Studies of High-Velocity Impact Fragmentation", Sandia National Laboratories Report, SAND93-0773, August 1993.

Kipp, M. E., R. R. Martinez, R. A. Benham, and S. H. Fischer (1999). "Explosive Containment Chamber Vulnerability to Chemical Munition Fragment Impact", Sandia National Laboratories Report SAND99-0189, February 1999.

Kipp, M. E. and R. R. Martinez (2000). "Assessment of Chemical Munition Fragment Impact in an Explosive Containment Chamber", Sandia National Laboratories Report SAND2000-0327, February 2000.

Kohn, B. J. (1969). "Compilation of Hugoniot Equations of State", Air Force Weapons Laboratory Report AFWL-TR-69-38, April 1969.

McGlaun, J. M., S. L. Thompson, and M. G. Elrick (1990). "CTH: A Three-Dimensional Shock Wave Physics Code", Int. J. Impact Engng., 10, 351-360.

MIL-HDBK-137 (1970). T244 Fuze Description. Personal communication from D. Benton, May 29, 2001.

Mock, W. and W. H. Holt (1983). "Fragmentation Behavior of Armco Iron and HF-1 Steel Explosive-Filled Cylinders", J. Appl. Phys., 54, 2344-2351.

Mott, N. F. (1943). "A Theory of the Fragmentation of Shells and Bombs", British Ministry of Supply Report A. C. 4035.

Old Chemical Weapons Reference Guide (1998). Published May 1998, Page 6-51.

Picatinny Arsenal (1961a). Drawing 8861029, Projectile, 155 mm, Gas, M121A1, Picatinny Arsenal Ordnance Corps, Department of the Army, Dover, New Jersey, November 1, 1961.

Picatinny Arsenal (1961b). Drawing 8861032, Burster, Projectile, M71, Picatinny Arsenal Ordnance Corps, Department of the Army, Dover, New Jersey, November 1, 1961.

Picatinny Arsenal (1961c). Drawing 8861031, Projectile, 155 mm, Gas, Persistent VX, M121A1, Filling Assembly, Picatinny Arsenal Ordnance Corps, Department of the Army, Dover, New Jersey, November 1, 1961.

Picatinny Arsenal (1961d). Drawing 8861030, Projectile, 155 mm, Gas, Non-Persistent GB, M121A1, Filling Assembly, Picatinny Arsenal Ordnance Corps, Department of the Army, Dover, New Jersey, November 1, 1961.

Picatinny Arsenal (1962). Drawing 10522519, Projectile, 8 inch, Gas, M426, Picatinny Arsenal Ordnance Corps, Department of the Army, Dover, New Jersey, October 30, 1962.

Silling, S. A. (1994). "Johnson-Cook Fracture Model Implementation in CTH", Sandia National Laboratories, Personal Communication.

Stofleth, J. H. (1999). Sandia National Laboratories, Personal Communication.

Stofleth, J. H. (2001). Sandia National Laboratories, Personal Communication.

Tennessee Valley Authority (2001). "Burster Detonation Vessel Report on Acceptance Testing Conducted in Karlskoga, Sweden April 18-19, 2001", Tennessee Valley Authority, April 26, 2001.

War Department (1918). Chemical Warfare Service Research Division, Liven's Projector, Drawing 44-G2_.

Whitney, M. G., G. J. Friesenhahn, W. E. Baker, and L. M. Vargas (1983). "A Manual to Predict Blast and Fragment Loadings from Accidental Explosions of Chemical Munitions Inside an Explosion Containment Structure", Volume I, Southwest Research Institue Report SwRI-6714, April 1983.

Wilson, L. T., D. R. Reedal, L. D. Kuhns, M. E. Kipp, and J. W. Black (2001). "Using a Numerical Fragmentation Model to Understand the Fracture and Fragmentation of Naturally Fragmenting Munitions of Differing Materials and Geometries", Proceedings, 19th International Symposium of Ballistics, Ed. I. R. Crewther, 7-11 May 2001, Interlaken, pp 671-678.

APPENDIX A - Material Model Parameters

The material parameters used in the exploding munition calculations are summarized in this appendix. The explosive parameters for Composition B (Table A1) are assumed to match those of Comp B Grade A explosive, for which JWL model parameters for the release product isentrope are available (Dobratz and Crawford, 1985). JWL model parameters for both the PETN and C-4 are from the same reference.

The equations of state for the inert materials present in the munition are listed in Table A2. These parameters are found in Group GMX-6 (1969). The spall stress for each material has also been included in this table. The solid materials were all treated with an elastic-perfectly plastic constant yield strength model. These parameters are listed in Table A3. The aluminum properties were extracted from Kohn (1969), the munition case steel properties were estimated from similar carbon steels (~1040-1050) and requirements stated on the drawings for the M121A1 (Picatinny Arsenal, 1962).

The fracture property sources were the same as those for the yield strengths. In addition, some use was made of the Johnson-Cook fracture model in CTH (Silling, 1994) to model the failure of the munition case in expansion. This model uses the extremes in fracture stress - from the initial spall stress to the uniaxial tensile stress at maximum elongation - to accommodate both high strain rate fracture accompanying relief wave interactions (spall) and much lower rate case expansion. The model is used with only pressure dependence,

$$\varepsilon_f = D_2 \cdot \exp(-D_3 P/Y) \qquad (A1)$$

where ε_f is the strain to failure, D_2 and D_3 are constants, P is the pressure, and Y is the yield strength. The parameters are listed in Table A4. The fragmentation model requires the fracture toughness for these materials. A range of possible toughnesses is listed in Table A4. A value of 265 MPa √m was used in the current calculations for the M121A1 munition case fragmentation in this document, leading to worst case (largest) fragments.

Table A1: JWL Material Model Parameters for Comp B Explosive

Parameter	Comp B	PETN	C-4
Density, ρ (g/cm^3)	1.717	1.770	1.601
Detonation Velocity (cm/s)	7.980×10^5	8.30×10^5	8.193×10^5
C-J Pressure (GPa)	29.5	33.5	28.0
Ideal Gas Constant, Γ	2.706	2.640	2.838
A (dynes/cm^2)	5.242×10^{12}	6.170×10^{12}	6.0977×10^{12}
B (dynes/cm^2)	7.678×10^{10}	1.6926×10^{11}	1.295×10^{11}
C (dynes/cm^2)	1.082×10^{10}	6.99×10^9	1.043×10^{10}
R_1	4.20	4.40	4.5
R_2	1.10	1.20	1.4
ω	0.34	0.25	0.25
C-J Temperature (eV)	0.35	0.35	0.35

Table A2: Equation of State Parameters for Inert Materials

Parameter	Aluminum (2024)	Steel (Iron)	Neoprene	Brass
Density (g/cm^3)	2.785	7.85	1.439	8.45
Sound Speed (cm/s)	5.328×10^5	3.574×10^5	2.785×10^5	3.726×10^5
Linear U_s-u_p Coefficient	1.338	1.92	1.419	1.434
Gruneisen Constant	2.00	1.69	1.39	2.04
Specific Heat (ergs/g/eV)	1.07×10^{11}	5.18×10^{10}	1.0×10^{10}	4.49×10^{10}
Spall Stress ($dynes/cm^2$)	-15.0×10^9	-39.0×10^9	-1.0×10^9	-14.0×10^9

Table A3: Yield Strength Parameters for Solid Materials

Parameter	Steel (M121)	Aluminum (2024)	Brass
Yield Stress ($dynes/cm^2$)	6.0×10^9	2.9×10^9	1.7×10^9
Poisson's Ratio	0.279	0.33	0.374
Melt Temperature (eV)	0.156	0.105	0.08

Table A4: Fracture Parameters for Munition Case

Parameter	Steel (M121)
Tensile Stress ($dynes/cm^2$)	6.8×10^9
Elongation (%)	15 - 30
D2 (J-C Coefficient)	0.163
D3 (J-C Coefficient)	-0.216
Fracture Toughness (MPa $\sqrt{m}$)	100 - 265
Sound Speed (cm/s)	4.6×10^5

APPENDIX B – Limit Velocity Curve Definition for 40 mm Target

An estimate of the limit velocity curve for the 40 mm wall of the Burster Detonation Vessel is made in this appendix, an extension of the work reported in Appendix C of Kipp, et al. (1999). In that appendix, both CTH impact simulations and an analytic penetration equation were used to establish a limit velocity curve for the 30 mm wall of the Explosive Containment Chamber. Here, only the penetration equation will be employed to provide the necessary boundary of fragment velocity versus fragment mass that determines the vulnerability of the vessel wall to the incident fragments presented in Tables 2 and 3 in the body of this report.

In Appendix C (Kipp, et al., 1999), the penetration equation relating target limit velocity, V_L, to long-rod projectile parameters for normal impact was put in the form,

$$V_L^{\,2} = \frac{A'}{r\left(L/D\right)}\left(t/D\right)^{1.6} \qquad \text{(B1)}$$

where t is the wall thickness, r is the projectile density, L is the projectile length, and D is the projectile diameter. The coefficient, A', is a constant calibrated to data for specific projectile and target performance. Several data points were employed in the referenced appendix to evaluate A', and values ranging from 7.8×10^{10} to 12.8×10^{10} dynes/cm^2 were derived from a few data sets. The density of steel is 7.8 g/cm^3, and the thickness of the target (BDV wall) is 4 cm (cgs units are being used in the equation in this application).

In order to apply Equation (B1), nominally rectangular fragments must be represented by a cylindrical rod geometry. Two possible choices (extremes) for the fragment in Figure B1 (left) are to convert its volume into a flat disk whose height is the fragment thickness, or into a rod whose length is the projectile length (Figure B1, right). In the latter, the impact of the fragment would be assumed on its edge, presumed to be the most damaging for perforation consequences. In addition, the penetration equation is calibrated for long rod impacts, not for flat disk impacts. The fragment cross-sectional area, formed by the thickness × width (shorter surface dimension), is converted to the diameter of a rod to be used in Equation B1, and the length of the fragment is retained as the rod length in Equation B1. Five fragments, covering most of the span of masses in Figure 17, are chosen as representative to define a limit velocity curve: fragments with masses 7, 35, 212, 800, and 2991 g and corresponding dimensions were selected from Tables 2 and 3 in the report. The 7 and 2991 g fragments are from Table 2, and the remaining fragments are drawn from Table 3.

Table B1 indicates the calculated equivalent rod diameter and the resulting limit velocity values for the two coefficient choices for A'. To some extent, these two choices represent the error bars associated with this method of determining the wall vulnerability. The smaller values for limit velocity would be considered the lower threshold for perforation of the 40 mm wall by the fragment.

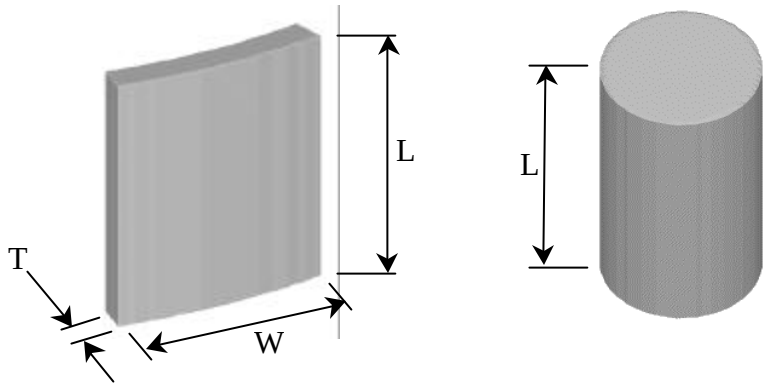

Figure B1. Fragment (left) and equivalent mass rod (right)

Table B1: Limit Velocities for Five Equivalent Fragments

Fragment Mass (g)	Original Fragment Dimensions			Equivalent Rod	Limit Velocity (m/s)	
	Length (cm)	Width (cm)	Thickness (cm)	Diameter (cm)	A' $7.8\text{x}10^{10}$	A' $12.8\text{x}10^{10}$
7	4.2	2.1	0.1	0.52	1800	2305
35	3.0	3.0	0.5	1.38	1590	2035
212	7.0	3.5	1.1	2.21	905	1155
800	10.36	5.18	1.9	3.54	645	825
2991	16.8	8.4	2.7	5.37	445	570

APPENDIX C – Summary of Previous Analyses of Other Chemical Munitions

In a previous report (Kipp and Martinez, 2000), fragmentation of four other munitions was considered in addition to the M121A1: Livens projectile, 4.2 inch mortar, Stokes mortar, and 75 mm Mk II chemical round. The expected fragments from both fully loaded with agent and drained configurations were determined. In this appendix, a summary is made of the estimated fragments from the drained munition calculations contained in Appendix C of that report. For purposes of comparison, all four rounds, along with the M121A1, are plotted in Figure C1 at the same scale, illustrating the wide range of geometries and sizes. Only the M121A1 is shown with a fuze in place. A summary of the burster charge and agent masses is in Table C1.

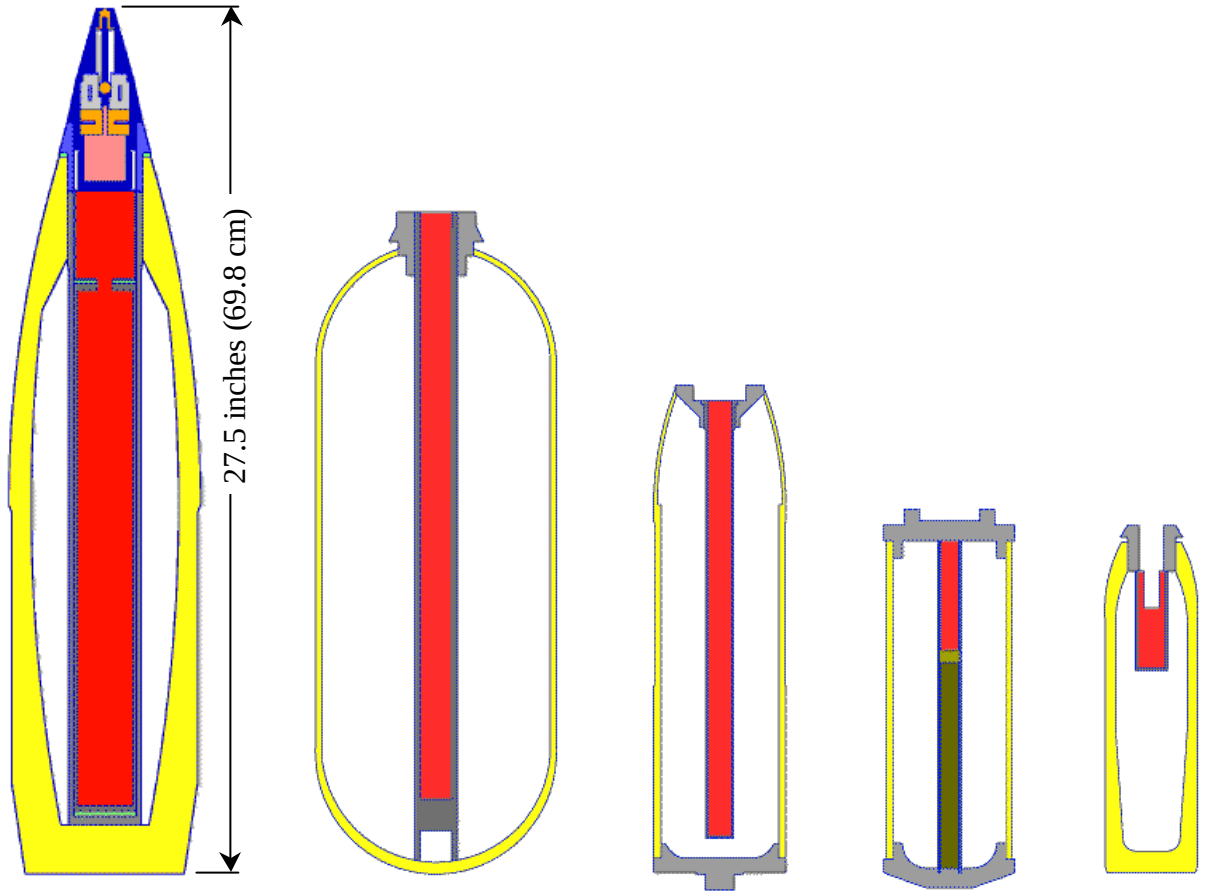

Figure C1. Scale comparison of five chemical munitions (all shown with agent drained): M121A1 155 mm, Livens projectile, 4.2 inch mortar, Stokes mortar, and 75 mm. (Munition case material is shown in yellow, explosive burster charge in red.)

The M121A1 is the most heavily cased of these five munitions, and contains the largest mass of explosive (1.26 kg), about 50 times more than that of the Stokes mortar. The Livens projectile carries the largest mass of agent (11 kg), which is nearly 25 times as much as contained in the 75 mm round.

Table C1: Summary of Projectile Explosive and Agent Masses

Munition	Burster Charge Mass (kg / lb.)	Agent Mass (kg / lb.)
M121A1, 155 mm	1.26 / 2.77	2.82 / 6.22
Livens Projectile	0.39 / 0.86	11.0 / 24.25
4.2 Inch Mortar	0.18 / 0.39	2.37 / 5.23
Stokes Mortar	0.025 / 0.06	1.56 / 3.43
75 mm Mk II	0.046 / 0.10	0.46 / 1.02

When the fragmentation of each of these additional four munitions (drained) was evaluated, the burster tube in the Livens, 4.2 inch mortar, and Stokes mortar, was expected to break up long before it reached the munition case. In that situation, it was deemed more appropriate to use cross-sections of these munitions to account for such behavior, where a fragment from the burster tube impacted the inside of the case, causing spall to occur. Out of those analyses, one average fragment size was determined from each munition that was used to represent the worst case fragment for the drained configuration. These fragments are summarized in Table C2.

Table C2: Fragment Masses and Velocities for Four Drained Munitions (from Appendix C, Kipp and Martinez, 2000)

Munition	Thickness (cm)	Width (cm)	Length (cm)	Fragment Mass (g)	Fragment Velocity (m/s)
Livens	0.35	1.0	15	40	700
4.2 inch Mortar	0.25	0.7	14	20	850
Stokes Mortar	0.15	1.4	10	15	680
75 mm Mk II	0.2	2.0	8	25	600

DISTRIBUTION

INTERNAL

MS 0612	Review and Approval Desk, 9612, For DOE/OSTI (1)
MS 0899	Technical Library, 9616 (2)
MS 9018	Central Technical Files, 8945-1
MS 0321	W. J. Camp, 9200
MS 0310	P. Yarrington, 9230
MS 0819	D. E. Carroll, 9231
MS 0820	G. C. Bessette, 9232
MS 0820	M. E. Kipp, 9232 (15)
MS 0820	S. A. Silling, 9232
MS 0820	P. A. Taylor, 9232
MS 0836	M. R. Baer, 9100
MS 0836	E. S. Hertel, 9116
MS 0847	J. W. Swegle, 9121
MS 1156	P. W. Cooper, 15322
MS 1156	D. S. Preece, 15322
MS 1156	W. V. Saul, 15322
MS 1156	J. H. Stofleth, 15322
MS 1453	R. A. Benham, 2553
MS 1454	M. C. Grubelich, 2554
MS 9004	J. Vitco, 8100
MS 9105	B. L. Haroldsen, 8118
MS 9105	J. E. Didlake, Jr., 8118
MS 9105	A. McDonald, 8118
MS 9105	K. L. Tschritter, 8119 (5)
MS 9161	E. P. Chen, 8726

EXTERNAL

Lt. Col. Christopher Ross
Product Manager for Non-Stockpile Chemical Materiel
ATTN: SFAE-CD-N, Bldg E4405
APG, MD 21010-4005

Donald R. Benton (5)
Non-Stockpile Chemical Materiel Program
ATTN: SFAE-CD-NP
Bldg E4410
Aberdeen PG, MD 21010-4005

William Brankowitz
Deputy PM, Non-Stockpile Chemical Materiel Program
ATTN: SFAE-CD-NP
Bldg E4405
APG, MD 21010-4005

Alan Caplan
Non-Stockpile Chemical Materiel Program
ATTN: SFAE-CD-NP
Bldg E4410
APG, MD 21010-4005

Ray DiBerardo
Non-Stockpile Chemical Materiel Program
ATTN: SFAE-CD-NP
Bldg E4410
APG, MD 21010-4005

M. Terry Frederick (2)
Non-Stockpile Chemical Materiel Program
ATTN: SFAE-CD-NP
Bldg E4510TA
APG, MD 21010-4005

Larry Gottschalk
Chief, Site Operations Team
Non-Stockpile Chemical Materiel Program
ATTN: SFAE-CD-NP
Bldg. E4410
APG, MD 21010-4005

Jerry Hawks
Non-Stockpile Chemical Materiel Program
ATTN: SFAE-CD-NP
Bldg E4410
APG, MD 21010-4005

Charles L. Heyman
Chief, System Operations Team
Non-Stockpile Chemical Materiel Program
ATTN: SFAE-CD-NM
Bldg. E4405
APG, MD 21010-4005

K. Kimsey
AMSRL WM TC
U. S. Army Research Laboratory
Aberdeen Proving Ground, MD 21005-5066

M. Lampson
AMSRL WM TC
U. S. Army Research Laboratory
Aberdeen Proving Ground, MD 21005-5066

Reina R. Martinez
P. O. Box 1663
Los Alamos, NM 87545

M. N. Raftenberg
AMSRL WM TD
U. S. Army Research Laboratory
Aberdeen Proving Ground, MD 21005-5066

W. Emerson Rudacille, Jr.
Project Engineer
Non-Stockpile Chemical Materiel Program
Post Office Box 216
APG, MD 21010-0216

Warren Taylor
Non-Stockpile Chemical Materiel Program
ATTN: SFAE-CD-NP
Bldg E4410
APG, MD 21010-4005

Commander
Dahlgren Division
Naval Surface Warfare Center
Attn: L. T. Wilson, Code G22
17320 Dahlgren Road
Dahlgren, VA 22448-5100